Summer 8-2010

Studies of Meson Mass Spectra in the Context of Quark-Antiquark Bound States

Mallika Dhar
University of Southern Mississippi

The University of Southern Mississippi

STUDIES OF MESON MASS SPECTRA IN THE CONTEXT OF QUARK-ANTIQUARK BOUND STATES

by

Mallika Dhar

Abstract of a Dissertation
Submitted to the Graduate School
of The University of Southern Mississippi
in Partial Fulfillment of the Requirements
for the Degree of Doctor of Philosophy

August 2010

ABSTRACT

STUDIES OF MESON MASS SPECTRA IN THE
CONTEXT OF QUARK-ANTIQUARK BOUND STATES

by Mallika Dhar

August 2010

This dissertation deals with the computation of meson mass spectra in the context of quark-antiquark ($q\bar{q}$) bound-state. Traditionally the $q\bar{q}$ bound-state problem is treated by solving the non-relativistic Schrödinger equation in position representation with a linear confining potential and a Coulomb-like attractive potential. For high energy, relativistic kinematics is necessary. It is well known that relativistic kinematics cannot be treated properly in position representation, but it can easily be handled in momentum representation. On the other hand, the linear potential and Coulomb-like potential have singularities in momentum-space and complicated subtraction procedure is necessary to treat the singularities properly. In order to deal with the double conflict, we have developed a method to solve any Schrödinger-like wave equation with/without relativistic kinematics in the mixed-space representation. In this representation, the kinematic term is treated in momentum-space and the potential term is treated in position-space. The results obtained from the mixed representation are in excellent agreement with the results obtained from the position-space and momentum space representations of the non-relativistic Schrödinger equation without the spin-dependent terms in potential. The success of our computational scheme encouraged us to extend the investigation towards relativistic treatment of the mesonic systems along with the spin-dependent interactions in potential. We have included relativistic kinematics and spin-dependent potentials along with the regular linear and Coulomb-type potentials in our equation. Our predicted results of meson masses are in excellent agreement with the experimental data.

The University of Southern Mississippi

STUDIES OF MESON MASS SPECTRA IN THE CONTEXT OF QUARK-ANTIQUARK BOUND STATES

by

Mallika Dhar

A Dissertation
Submitted to the Graduate School
of The University of Southern Mississippi
in Partial Fulfillment of the Requirements
for the Degree of Doctor of Philosophy

Approved:

Dr. Khin Maung Maung

Director

Dr. John Norbury

Dr. Lawrence Mead

Dr. Christopher Sirola

Dr. Sung Lee

Dr. Susan A. Siltanen

Dean of the Graduate School

August 2010

ACKNOWLEDGMENTS

I would like to thank all of those who have assisted me in this effort. I am forever thankful to my adviser, Dr. Khin Maung Maung, who taught me with great patience and helped me in many ways to complete my dissertation. He taught me with great care and helped me to understand the nature of research in the field of theoretical physics and computations. I have gained considerable amount of knowledge and experience while working under his supervision. I would like to thank my other committee members, Dr. John Norbury, Dr. Lawrence Mead, Dr. Sung Lee and Dr. Christopher Sirola, whose active support made it possible for me to complete my dissertation. I would like to thank my friend Charles Werneth with all my heart; without his active support, both academically and emotionally, it would not have been possible for me to carry on. I would like to thank my parents, Sarashi Ranjan Dhar and Manju Dhar, for their kindness, love and care. They are always very supportive. I would like to thank my brother, Tanmay Dhar, for his continuous support and care.

TABLE OF CONTENTS

LIST OF ILLUSTRATIONS

Figure

LIST OF TABLES

Table

LIST OF ABBREVIATIONS

A& S	-	Abramowitz and Stegun
HO	-	Harmonic Oscillator
NRSE	-	Nonrelativistic Schrödinger Equation
QCD	-	Quantum Chromodynamics
QED	-	Quantum Electrodynamics

NOTATION AND GLOSSARY

General Usage and Terminology

The notation used in this text represents fairly standard mathematical and computational usage. In many cases these fields tend to use different preferred notation to indicate the same concept, and these have been reconciled to the extent possible, given the interdisciplinary nature of the material.

The capital letters with tilde, $\tilde{H}, \tilde{D}, \cdots$ are used to denote matrices.The capital letters with tilde and two indices, $\tilde{H}_{ij}$ are used to denote matrix elements. Letters with right angles, $|\phi\rangle, |\psi\rangle$ are used to denote the ket vectors. Letters with left angles, $\langle\phi|, \langle\psi|$ are used to denote the bra vectors. Letters with hats, $\hat{H}$, $\hat{T}$, $\hat{p}$ are used to denote the operators. Lower case letters such as $i, j, k, l, m, n, \alpha, \beta$ are used to denote indices.

Chapter 1

BACKGROUND

1.1 Introduction

According to the quark model, a quark is the fundamental building block of matter. A meson is a two-body bound state of a quark and an antiquark. Quarks and antiquarks are subject to the strong interaction. The theory which describes the mechanism of the strong interaction is known as Quantum Chromodynamics(QCD). According to QCD, quarks and antiquarks interact by exchanging gauge bosons called gluons. Lattice gauge calculations indicate that the interaction between a quark and an antiquark could very well be approximated by a linear plus a Coulomb-type potential. The linear part of the potential models the *confinement* and Coulomb-part models *asymptotic freedom* [4]. These two important properties:*confinement* and *asymptotic freedom* will be discussed later(Section 1.2).

The quark-antiquark($q\bar{q}$) pair has discrete energy levels corresponding to the different modes of $q\bar{q}$ excitations, rotations, vibrations etc. [5] These discrete energy levels must correspond to the observed meson states.

The main motivation of this dissertation is to produce meson mass spectra in the context of quark-antiquark ($q\bar{q}$) bound states. A brief overview of the quark model and Quantum Chromodynamics(QCD) is given in the next section.

1.2 Brief Overview

A large number of new particles were discovered from the particle accelerator experiments in 1960's [6]. Soon, it became clear that they could not be elementary. Gell-Mann [7] and Zweig [8] provided a simple idea which solved the problem. They proposed that the fundamental building block of matter is the quark. Each meson is a two-body bound state of a quark and an antiquark and each baryon is a three-body bound state of three quarks. For example, the meson known as J/Ψ is a bound state of charm (c) and anticharm ($\bar{c}$) quarks. The proton is a baryon; it is a three-body bound state of two up (u) quarks and one down (d) quark and a neutron is a three-body bound state of one up (u) quark and two down (d) quarks.

It is now widely accepted that there are six flavors of quarks: up(u), down(d), strange(s), charm(c), bottom(b) and top(t). Each quark carries fractional electric charge: up(u), charm(c) and top(t) quarks have charge $+\frac{2}{3}$e and down(d), strange(s) and bottom(b) quarks have charge $-\frac{1}{3}$e. A complete list of quarks with their electric charges are presented in Table 1.1.

Table 1.1: A List of Quarks and Their Electric Charges

Flavor	Symbol	Electric Charge (e)
up	u	$+\frac{2}{3}e$
down	d	$-\frac{1}{3}e$
charm	c	$+\frac{2}{3}e$
strange	s	$-\frac{1}{3}e$
top	t	$+\frac{2}{3}e$
bottom	b	$-\frac{1}{3}e$

In addition to electric charge, quarks have a property known as color charge. This property was introduced in 1964 by Greenburg [9] and in 1965 by Han and Nambu[10]. Color charge is a fundamental property of quarks and antiquarks. Quarks come in three primary colors, denoted as R, G and B. Antiquarks are assigned with complementary colors $\bar{R}$, $\bar{G}$ and $\bar{B}$. This "color" has no relation to the real colors of everyday life, this color charge is simply a quantum property.

Quarks and antiquarks combine together to form hadrons(mesons and baryons) in such a way that all observed hadrons are colorless(color singlet) and carry integer electric charge. This theoretical description works well because all the quark bound states that are detected in various experiments are all colorless(color singlet).[5]

All modern theories of interactions are gauge theories. According to gauge theory, each of the interactions between various particles is due to the exchange of gauge bosons. For example, electromagnetic interaction is caused by the exchange of photons between the charged particles. The theory that describes electromagnetic interaction is known as Quantum Electrodynamics(QED).

By analogy with Quantum Electrodynamics (QED), in which photons are the exchange particles of the electromagnetic interaction, particles known as *gluons* are the exchange particles of the strong interaction. Gluons are exchanged between the particles with color charge. The important difference between QED and QCD is that unlike photons which are chargeless, gluons carry color charges. Since each gluon carries color charge, they interact with one another [11] [12]. This leads to the fact that gluons in the system behave in such a way that the magnitude of the interaction potential increases as the distance between the interacting particles increases. This property is known as anti-screening. In Figure(1.1), a pictorial description is given about the difference between the Quantum Electrodynamics (QED) and Quantum Chromodynamics (QCD) [5]. Notice that effective color charge increases as the distance increases from the color-charged particle and the effective electric charge decreases as the distance increases from the electrically charged particle.

Anti-screening is the cause of the important phenomenon known as *asymptotic freedom* [4].

Asymptotic freedom suggests that at short distance (high energy) strongly interacting particles behave as if they are asymptotically free; their effective coupling is very weak at very short distance. On the other hand, the effective coupling between the strongly interacting particles is very large at large distance(low energy) which gives rise to confinement.

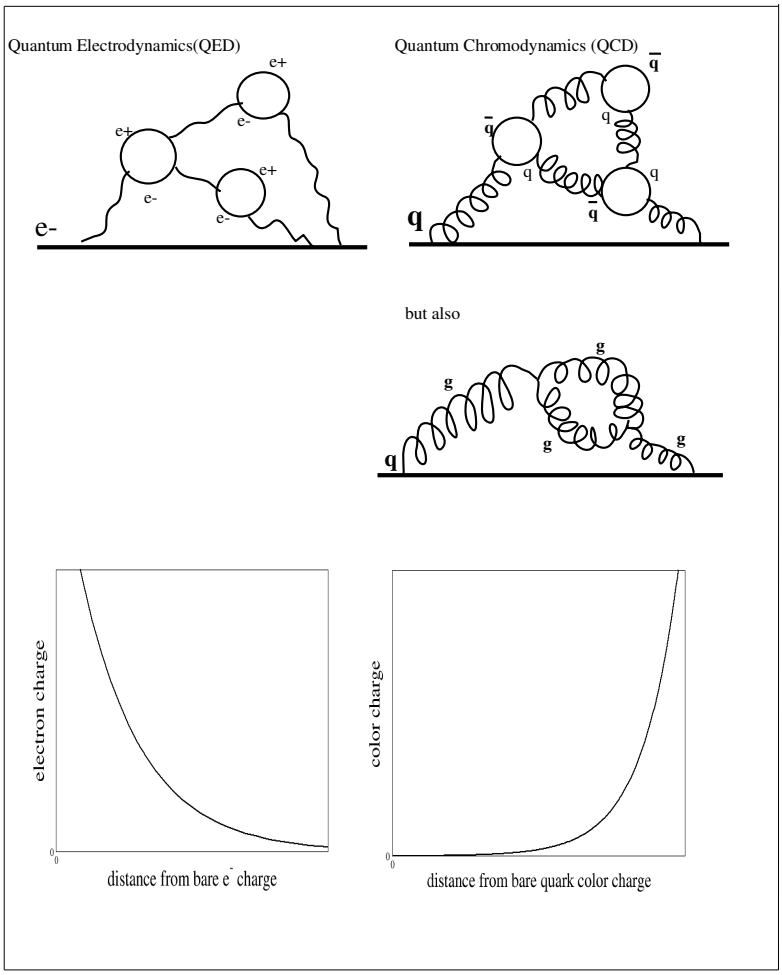

Figure 1.1: This is the pictorial description of the difference between the Quantum Electrodynamics (QED) and Quantum Chromodynamics (QCD). In QED, the exchange particle is photon, they do not interact with each other. The effective electric charge decreases as the distance increases from the electrically charged particle. In QCD, the exchange particle is gluon, they interact with one another. As a result, gluons cause anti-screening which gives rise to the property of asymptotic freedom. Each quark has color charge, effective color charge increases as the distance from the quark increases.

Asymptotic freedom was introduced in 1973 by Gross and Wilczec [4] and Politzer [13]. This is a very important and useful property to study the high energy behavior of QCD. Because

of asymptotic freedom, the strong coupling constant is small for sufficiently small distances and amenable to perturbative method. The one gluon exchange model was used successfully to model the very small distance interactions of quarks [14].

Another important property of strong interaction is known as *confinement*. Quarks are forever bound inside either a two-body system called a meson or a three-body system called a baryon. Free quarks in nature have never been experimentally observed. To explain the complete absence of an isolated quark, it is said that the color-charged particles cannot be isolated. If one tries to isolate a quark, at some point it becomes energetically more favorable for a new quark/antiquark pair to be created out of the vacuum than to allow the quarks to separate farther.

Lattice gauge calculations and Wilson loop calculations show that for large distances the potential between the quarks exhibit linear behavior[11] [15][16] [17] [18] [19]. As a result, confinement appears as a property of QCD.

1.3 Models of Quantum Chromodynamics (QCD)

Quantum Chrmodynamics (QCD) was proposed in 1970's as a theory of the strong interactions. It was widely accepted after the discovery of asymptotic freedom in 1973. QCD offered a satisfactory explanation of some of the puzzling experimental results at that time. Since then, QCD continued to succeed in explaining the physics of strong interaction. [20]

QCD is especially successful in the high energy region. Effective methods derived from the first principles have been developed for the high energy region. However, properties of medium and low energy QCD is still a challenge and remains an open research area. Perturbation theory is not applicable in low and medium energy region and no other rigorous analytical method has been developed so far.[15]

One way is to invent models to capture the most important features of QCD. A great variety of models have been developed. Those models are quenched lattice gauge theory, The Dyson-Schwinger formalism, constituent quark models, light cone QCD and various effective field theories. [21] [22]

Of all these models, we have chosen the constituent quark model in our studies of meson mass spectra. In the constituent quark model, the gluon degrees of freedom are eliminated in favor of confined constituent quarks with effective masses coming from chiral symmetry breaking and quark-antiquark effective interactions. [23][24]

To start our studies of meson mass spectra, we began with a two-body Schrödinger equation. In the next section, the two-body Schrödinger Equation is described.

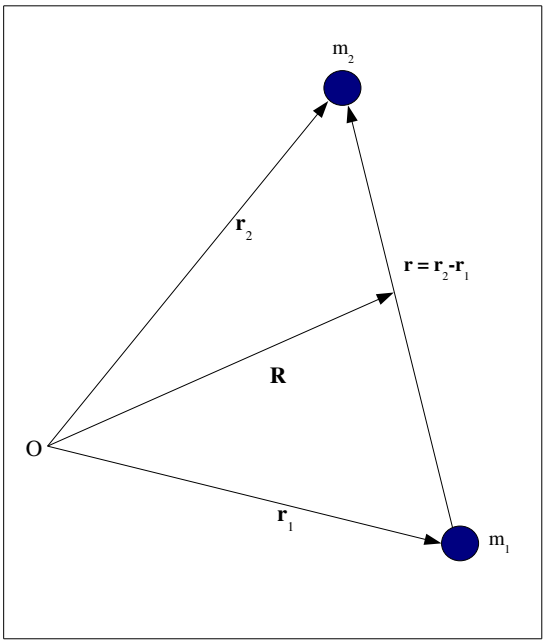

Figure 1.2: Diagram depicting center of mass and relative coordinates.

1.4 The Two-Body Schrödinger Equation

We are interested in investigating the meson mass spectra in the context of quark-antiquark($q\bar{q}$) bound states. To do that, we need to solve the time-independent Schrödinger-type equation with and without relativistic kinematics. [25] In this section we briefly describe how center of mass motion and relative motion are separated out.

The time-independent Schrödinger equation for a two particle system with a central potential $V(r)$ can be written as the following:

$$\Big[\frac{\mathbf{p}_1^2}{2m_1}+\frac{\mathbf{p}_2^2}{2m_2}+V(r)\Big]\Psi(\mathbf{r}_1,\mathbf{r}_2)=E\Psi(\mathbf{r}_1,\mathbf{r}_2), \tag{1.1}$$

where m_1 is the mass of particle 1 and m_2 is the mass of particle 2 and the relative distance = $\mathbf{r}\equiv\mathbf{r_2}-\mathbf{r_1}$. If we separate the relative motion and the motion of the center of mass, then the above equation can be rewritten as the following:

$$\Big[\frac{\mathbf{P^2}}{2M}+\frac{\mathbf{p^2}}{2\mu}+V(r)\Big]\Psi(R,r)=E\Psi(R,r), \tag{1.2}$$

where $\mathbf{P}$ = total momentum = $\mathbf{p}_1 + \mathbf{p}_2$, $\mathbf{p}$ = relative momentum = $\frac{m_2\mathbf{p_1} - m_1\mathbf{p_2}}{m_1+m_2}$, M = total mass= $m_1 + m_2$, μ = reduced mass = $\frac{m_1 m_2}{m_1+m_2}$ and $\mathbf{r}$ = relative distance between particle 1 and particle 2 = $\mathbf{r}_2 - \mathbf{r}_1$ Now we write

$$E = E_{cm} + E_{rel}, \tag{1.3}$$

where E_{cm} is the center of mass energy and E_{rel} is the relative energy. After the separation of variables in center of mass and relative coordinates, the Schrödinger equation in relative coordinates can be written as

$$\left[\frac{\mathbf{p^2}}{2\mu} + V(r)\right]\Psi(r) = E_{rel}\Psi(r). \tag{1.4}$$

Note that the potential between the two particles depends only on the relative distance.

In Figure 1.2, a schematic diagram of the center of mass and relative coordinates are given. The two-body Schrödinger equation, could be expressed in position space, momentum space and mixed space representations. In the following chapters we will discuss about those representations and the solution methods.

Chapter 2

THE SCHRÖDINGER EQUATION IN POSITION REPRESENTATION

2.1 The Schrödinger Equation of a Two-Body Bound State in Position-Space

The Schrödinger equation is usually solved in position-space. Let's present a short derivation of the position-space representation of the Schrödinger equation here. Since we are interested only in the relative motion equation (1.4), all the quantities correspond to relative variables.
We start from the Schrödinger equation in Hilbert space,

$$\hat{H}|\Psi_n\rangle = E_n|\Psi_n\rangle. \tag{2.1}$$

The eigenstates $|\Psi_n\rangle$ make a complete orthonormal set of eigenstates in Hilbert space. Hamiltonian operator $\hat{H}$ can be written as a sum of the relative kinetic energy operator $\hat{T}$ and the potential energy operator $\hat{V}$. So, we have

$$[\hat{T}+\hat{V}]|\Psi_n\rangle = E_n|\Psi_n\rangle. \tag{2.2}$$

By projecting this equation on position-space basis :

$$\langle\mathbf{r}|[\hat{T}+\hat{V}]|\Psi_n\rangle = E_n\langle\mathbf{r}|\Psi_n\rangle. \tag{2.3}$$

The non-relativistic kinetic energy operator is expressed as

$$\hat{T} = \frac{\hat{p}^2}{2\mu}, \tag{2.4}$$

where $\hat{p}$ is the relative momentum operator and $\mu = \frac{m_1 m_2}{m_1+m_2}$ is the reduced mass of the two-body system of mass m_1 and m_2.
The position basis matrix element of the quantum mechanical momentum operator $\hat{p}$ is:

$$\langle\mathbf{r}|\hat{p}|\mathbf{r}'\rangle = -i\hbar\nabla_r\delta(\mathbf{r}-\mathbf{r}'), \tag{2.5}$$

Inserting position completeness and using the relation given above, we can write the Schrödinger equation as the following,

$$\frac{-\hbar^2}{2\mu}\nabla^2\psi_n(\mathbf{r}) + \int\langle\mathbf{r}|\hat{V}|\mathbf{r}'\rangle\langle\mathbf{r}'|\psi_n\rangle d\mathbf{r}' = E_n\psi_n(\mathbf{r}). \tag{2.6}$$

Equation(2.6) is the most general form of the Schrödinger equation in position space. It is an integro-differential equation with a non-local potential $\langle\mathbf{r}'|\hat{\mathbf{V}}|\mathbf{r}\rangle$. If the potential is a local potential, then

$$\langle\mathbf{r}|\hat{V}|\mathbf{r}'\rangle = V(r)\delta(\mathbf{r}-\mathbf{r}'). \tag{2.7}$$

Using the property of a local potential, we can write

$$\frac{-\hbar^2}{2\mu}\nabla^2\psi_n(\mathbf{r}) + \int V(r)\delta(\mathbf{r}-\mathbf{r}')\psi_n(\mathbf{r}')d\mathbf{r}' = E_n\psi_n(\mathbf{r}). \tag{2.8}$$

Using the delta function we integrate and obtain the following:

$$\frac{-\hbar^2}{2\mu}\nabla^2\psi_{nl}(\mathbf{r}) + V(r)\psi_{nl}(\mathbf{r}) = E_n\psi_{nl}(\mathbf{r}). \tag{2.9}$$

Equation(2.9) is the position-space representation of the Schrödinger equation. If the orbital angular momentum $\vec{\mathbf{L}}$ is good quantum number, we can separate the variables in radial and angular parts as

$$\psi_{nl}(\mathbf{r}) = \frac{U_{nl}(r)}{r}Y_l^m(\hat{r}), \tag{2.10}$$

where $U_{nl}(r) = r\psi_{nl}(r)$ is the reduced wave function, r is the relative distance between the two particles, $Y_l^m(\hat{r})$ is the spherical harmonic and $\hat{r}$ is the unit vector along the direction of $\mathbf{r}$. After separating the angular variables, the Schrödinger equation becomes:

$$\frac{-\hbar^2}{2\mu}\frac{d^2}{dr^2}U_{nl}(r) + V(r)U_{nl}(r) + \frac{\hbar^2}{2\mu}\frac{l(l+1)}{r^2}U_{nl}(r) = E_nU_{nl}(r). \tag{2.11}$$

The normalization of $U_{nl}(r)$ is given by

$$\int_0^\infty |U_{nl}(r)|^2 dr = 1. \tag{2.12}$$

Equation (2.11) is the radial part of the Schrödinger equation in position space.

Chapter 3

THE SCHRÖDINGER EQUATION IN MOMENTUM REPRESENTATION

3.1 Momentum Representation of the Two-Body Schrödinger Equation

For high energy quantum systems, relativistic kinematics is necessary. In order to treat relativistic kinematics properly, the Schrödinger equation is solved in momentum-space.

We will first present a short derivation of the Schrödinger in the momentum representation. In Hilbert space,

$$\hat{H}|\Phi_n\rangle = E|\Phi_n\rangle. \tag{3.1}$$

Since, $\hat{H} = \hat{T} + \hat{V}$, above equation becomes

$$(\hat{T} + \hat{V})|\Phi_n\rangle = E|\Phi_n\rangle, \tag{3.2}$$

where $\hat{T} = \frac{\hat{p}^2}{2\mu}$, for non-relativistic case and $\hat{T} = \sqrt{\hat{p}^2 + m_1^2} + \sqrt{\hat{p}^2 + m_2^2}$ for relativistic case. $\hat{V}$ is the operator for the potential and $\mu = \frac{m_1 m_2}{m_1 + m_2}$ = reduced mass of the two-body system of mass m_1 and m_2.
After projecting with $\langle \mathbf{p}|$ from the left we obtain the following:

$$\langle \mathbf{p}|\hat{T}|\Phi_n\rangle + \langle \mathbf{p}|\hat{V}|\Phi_n\rangle = E\langle \mathbf{p}|\Phi_n\rangle. \tag{3.3}$$

We insert a momentum-space completeness in the first and second term to obtain the following form:

$$\int \langle \mathbf{p}|\frac{\hat{p}^2}{2\mu}|\mathbf{p}'\rangle\langle \mathbf{p}'|\Phi_n\rangle d\mathbf{p}' + \int \langle \mathbf{p}|\hat{V}|\mathbf{p}'\rangle\langle \mathbf{p}'|\Phi_n\rangle d\mathbf{p}' = E\langle \mathbf{p}|\Phi_n\rangle. \tag{3.4}$$

When there is no coupling between angular momenta we can write

$$\Phi_n(\mathbf{p}) = \phi_{nl}(p)Y_l^m(\hat{p}). \tag{3.5}$$

and the momentum-space potential can be expressed as

$$\langle \mathbf{p}|\hat{V}|\mathbf{p}'\rangle = \sum_{l=0}^{\infty}\sum_{m=-l}^{l} V_l(p,p')Y_l^m(\hat{p})Y_l^{*m}(\hat{p}'). \tag{3.6}$$

Now using the separation of variables and integrating the angular parts, we obtain the Schrödinger equation for the l^{th} partial wave as the following:

$$\frac{p^2}{2\mu}\phi_{nl}(p) + \int_0^{\infty} V_l(p,p')\phi_{nl}(p')p'^2 dp' = E_{nl}\phi_{nl}(p), \tag{3.7}$$

where $p = |\mathbf{p}|$, n is the principal quantum number and l is the orbital angular momentum quantum number. This equation (3.7) is the 1-D momentum-space representation of the Schrödinger equation for ϕ_{nl}. The partial-wave components of the potential are readily obtained as

$$V_l(p,p') = 2\pi \int_{-1}^{+1} V(\mathbf{q}) P_l(x) dx, \tag{3.8}$$

where $P_l(x)$ is the Legendre polynomial of the first kind, $x \equiv \cos\theta_{pp'}$ and $\theta_{pp'}$ is the angle between vectors $\mathbf{p}$ and $\mathbf{p}'$ and $V(\mathbf{q})$ is the momentum-space potential where $\mathbf{q} = \mathbf{p}' - \mathbf{p}$.

If we start from a power-law potential in position-space

$$V(r) = \lambda_N \lim_{\eta \to 0} r^N e^{-\eta r}, \tag{3.9}$$

where λ_N is the strength of the potential and η is the screening parameter. The index N indicates the type of potential under consideration, $N = -1$ corresponds to the Coulomb-like potential and $N = 1$ corresponds to the linear potential.

The momentum space potential $V(\mathbf{q})$ can be expressed as the Fourier transform of the power-law potential in position-space as equation(3.9):

$$V^N(\mathbf{q}) = \frac{\lambda_N}{2\pi^2} \lim_{\eta \to 0} (-1)^{N+1} \frac{\partial^{N+1}}{\partial \eta^{N+1}} \left[\frac{1}{\mathbf{q}^2 + \eta^2} \right]. \tag{3.10}$$

Using this expression of $V(\mathbf{q})$ in equation(3.8) we can express the partial-wave component of the potential as

$$V_l(p,p') = \frac{\lambda_N}{\pi} \lim_{\eta \to 0} (-1)^{N+1} \frac{\partial^{N+1}}{\partial \eta^{N+1}} \frac{Q_l(y)}{pp'}, \tag{3.11}$$

where $y = \frac{p^2 + p'^2 + \eta^2}{2pp'}$ and $Q_l(y)$ is the Legendre polynomial of the second kind. We'll see that the quantity $V_l(p,p')$ for the linear potential and the Coulomb potential have singularities. For the Coulomb potential,

$$V_l^C(p,p') = \frac{\lambda_C}{\pi} \lim_{\eta \to 0} \frac{Q_l(y)}{pp'}. \tag{3.12}$$

and for the linear potential,

$$V_l^L(p,p') = \frac{\lambda_L}{\pi} \lim_{\eta \to 0} \frac{\partial^2}{\partial \eta^2} \frac{Q_l(y)}{pp'} = \frac{\lambda_L}{\pi} \lim_{\eta \to 0} \left[\frac{Q_l'(y)}{(pp')^2} + \frac{\eta^2}{(pp')^3} Q_l''(y) \right], \tag{3.13}$$

These potentials in equation(3.12) and in equation(3.13) have singularities (at $\eta = 0$) when $p = p'$. In order to show the singularity structure clearly, we write $Q_l(y)$ in terms of $Q_0(y)$ as the following:

$$Q_l(y) = P_l(y) Q_0(y) - w_{l-1}(y), \tag{3.14}$$

where $w_{l-1}(y) = \sum_{m=1}^{l} \frac{1}{m} P_{l-m}(y) P_{m-1}(y)$. In the expression of $Q_l(p)$, the singularity occur in the term $Q_0(y)$ at $\eta = 0$. We see that

$$Q_0(y) = \frac{1}{2} ln \left| \frac{y+1}{y-1} \right|. \tag{3.15}$$

and

$$Q_0'(y) = \frac{1}{1-y^2} = pp' \left[\frac{-1}{(p'-p)^2+\eta^2} + \frac{1}{(p'+p)^2+\eta^2} \right]. \tag{3.16}$$

and

$$\frac{\eta^2}{pp'} Q_0''(y) = \eta^2 (p^2 + p'^2 + \eta^2) \left[\frac{-1}{(p'-p)^2+\eta^2} + \frac{1}{(p'+p)^2+\eta^2} \right]. \tag{3.17}$$

So, we see that the Coulomb potential has a logarithmic singularity from $Q_0(y)$ and the linear potential has higher order singularities coming from $Q_0'(y)$ and $Q_0''(y)$. Note that $Q_0'(y)$ is a derivative with respect to y. We can take care of these singularities by a subtraction method invented by other researchers. [25] [26] [27] [28] [29]

Chapter 4

THE SCHRÖDINGER EQUATION IN MIXED REPRESENTATION

4.1 The Schrödinger Equation in Mixed-Space

The Schrödinger Equation can be expressed as a form where kinetic energy part of the equation is expressed in momentum space and potential energy part is expressed in position space.[30] [31] [32] [33] [34] [35] [36] .

By treating the potential term in position space we are able to avoid the singularities associated with the linear and Coulomb potentials in momentum-space.

We will first present a short derivation of the Schrödinger in the mixed representation. In Hilbert space,

$$(\hat{T}+\hat{V}|\Psi\rangle = E|\Psi\rangle \tag{4.1}$$

where $\hat{T}$ is $\frac{\hat{p}^2}{2\mu}$, for non-relativistic case and $\hat{T}$ is $\sqrt{\hat{p}^2+m_1^2}+\sqrt{\hat{p}^2+m_2^2}$ for relativistic case. $\hat{V}$ is the operator for the potential and $\mu = \frac{m_1 m_2}{m_1+m_2}$ = reduced mass of the two-body system of mass m_1 and m_2.
After projecting with $\langle\mathbf{p}|$ from the left we obtain the following:

$$\langle\mathbf{p}|\hat{T}|\Psi\rangle + \langle\mathbf{p}|\hat{V})|\Psi\rangle = E\langle\mathbf{p}|\Psi\rangle \tag{4.2}$$

We insert momentum completeness in the first term and two position-space completenesses in the second term to obtain the following form:

$$\int\langle\mathbf{p}|\frac{\hat{p}^2}{2\mu}|\mathbf{p}'\rangle\langle\mathbf{p}'|\Phi_n\rangle d\mathbf{p}' + \int\int\langle\mathbf{p}|\mathbf{r}\rangle\langle\mathbf{r}|\hat{V})|\mathbf{r}'\rangle\langle\mathbf{r}'|\Psi\rangle d\mathbf{r}d\mathbf{r}' = E\langle\mathbf{p}|\Psi\rangle \tag{4.3}$$

Using the definition of the plane wave i.e.

$$\langle\mathbf{p}|\mathbf{r}\rangle = \frac{1}{(2\pi)^{3/2}}\int e^{-i\mathbf{p}\cdot\mathbf{r}} \tag{4.4}$$

and the definition of a local potential i.e. $\langle\mathbf{r}|\hat{V}|\mathbf{r}'\rangle = V(r)\delta(\mathbf{r}-\mathbf{r}')$ we obtain

$$\frac{\mathbf{p}^2}{2\mu}\Phi(\mathbf{p}) + \frac{1}{(2\pi)^{3/2}}\int e^{-i\mathbf{p}\cdot\mathbf{r}}V(r)\Psi(\mathbf{r})d\mathbf{r} = E\Phi(\mathbf{p}) \tag{4.5}$$

Here $\Phi(\mathbf{p})$ is the Fourier transform of the r-space wave function $\Psi(\mathbf{r})$ and is given by

$$\Phi(\mathbf{p}) = \frac{1}{(2\pi)^{3/2}}\int e^{-i\mathbf{p}\cdot\mathbf{r}}\Psi(\mathbf{r})d\mathbf{r} \tag{4.6}$$

When there is no coupling between angular momenta we can write $\Psi(\mathbf{r}) = \psi_{nl}(r)Y_l^m(\hat{r})$ and $\Phi(\mathbf{p}) = \phi_{nl}(p)Y_l^m(\hat{p})$. Now using this angular separation, expanding the plane-wave and after performing the angular integration, we obtain

$$\frac{\mathbf{p}^2}{2\mu}\phi_{nl}(p) + \sqrt{\frac{2}{\pi}}\int_0^\infty j_l(pr)V(r)\psi_{nl}(r)r^2dr = E\phi_{nl}(p) \tag{4.7}$$

and $\phi_{nl}(p)$ and $\psi_{nl}(r)$ are related by a Fourier-Bessel transform given by

$$\phi_{nl}(p) = \sqrt{\tfrac{2}{\pi}}\int_0^\infty j_l(pr)\psi_{nl}(r)r^2dr \tag{4.8}$$

$$\psi_{nl}(r) = \sqrt{\tfrac{2}{\pi}}\int_0^\infty j_l(pr)\phi_{nl}(p)p^2dp \tag{4.9}$$

In the last two equations(4.9), we have absorbed a factor of $(-i)^l$ into the definition of $\psi_{nl}(r)$. Equation (4.7) is the Schrödinger equation in the mixed representation. In the next section we will discuss how to solve this equation by using the variational method.

Chapter 5

THE VARIATIONAL METHOD

5.1 Solving the Schrödinger Equation Using the Variational Principle

The Schrödinger equation in Hilbert space is written as

$$\hat{H}|\psi\rangle = E|\psi\rangle \tag{5.1}$$

where $\hat{H}$ is the Hamiltonian operator, E is the energy eigen value and $|\psi\rangle$ is the state vector. The variational method is remarkably successful in the calculation of the approximate solutions to the Schrödinger equation. We suppose that $|\psi\rangle$ is an arbitrary trial state which gives an approximate solution to the Schrödinger equation. Let E be an energy defined by

$$E = \frac{\langle\psi|\hat{H}|\psi\rangle}{\langle\psi|\psi\rangle} \tag{5.2}$$

We can write $|\psi\rangle$ as a linear combination of the basis states as the following:

$$|\psi\rangle = \sum_{j=1}^{\infty} c_j|g_j\rangle \tag{5.3}$$

where c_j are the coefficients and $|g_j\rangle$ are the basis states. Since the basis states are not necessarily orthogonal to each other, we can write

$$\langle g_i|g_j\rangle = D_{ij} \tag{5.4}$$

Now substituting Equation(5.3) into Equation(5.2), we obtain the following

$$E\sum_{i=1}^{\infty}\sum_{j=1}^{\infty} c_i^* c_j\langle g_i|g_j\rangle = \sum_{i=1}^{\infty}\sum_{j=1}^{\infty} c_i^* c_j\langle g_i|\hat{H}|g_j\rangle \tag{5.5}$$

Now we differentiate both sides of the Equation (5.5) with respect to one of the coefficients, c_k^* and we obtain the following:

$$\frac{\partial E}{\partial c_k^*}\sum_{i,j}^{\infty} c_i^* c_j D_{ij} + E\sum_{j}^{\infty} c_j D_{kj} = \sum_{j}^{\infty} c_j\langle g_k|\hat{H}|g_j\rangle \tag{5.6}$$

A stationary value of the energy could be obtained by setting

$$\frac{\partial E}{\partial c_k^*} = 0 \tag{5.7}$$

Now we can see

$$\sum_{j=1}^{\infty} H_{kj}c_j - E\sum_{j=1}^{\infty} D_{kj}c_j = 0 \tag{5.8}$$

where $H_{kj} = \langle g_k|\hat{H}|g_j\rangle$. We can write Equation(5.8) as

$$\sum_{j=1}^{\infty} H_{kj}c_j = E\sum_{j=1}^{\infty} D_{kj}c_j \tag{5.9}$$

When the process is repeated for other coefficients, additional equations of the type of Equation(5.9) are obtained and the number of such equations are equal to the number of basis functions in Equation (5.3). In principle, infinite number of basis should be used to construct the trial wavefunction. In practice, we can not use infinite number of basis; we use a finite number of basis. To compensate the truncation, we use a variational parameter in our basis. These system of equations gives us the matrix eigenvalue equation like the following:

$$\begin{pmatrix} H_{11} & H_{12}\cdots H_{1n} \\ H_{21} & H_{21}\cdots H_{2n} \\ \vdots & \\ H_{n1} & H_{n2}\cdots H_{nn} \end{pmatrix} \begin{pmatrix} c_1 \\ c_2 \\ \vdots \\ c_n \end{pmatrix} = E \begin{pmatrix} D_{11} & D_{12}\cdots D_{1n} \\ D_{21} & D_{21}\cdots D_{2n} \\ \vdots & \\ D_{n1} & D_{n2}\cdots D_{nn} \end{pmatrix} \begin{pmatrix} c_1 \\ c_2 \\ \vdots \\ c_n \end{pmatrix} \tag{5.10}$$

We can write the above equation in short form like the following:

$$\tilde{D}^{-1}\tilde{H}c = Ec \tag{5.11}$$

This Equation(5.11) is a standard matrix eigenvalue problem and can be solved for a given value of the variational parameter b in the basis function $g_j(r,b)$. [37] [38] [39] [40]

5.2 Solution in Position-Space

We do our computations using three different sets of basis functions independently. We use Gaussian, exponential, and Laguerre basis for the expansion in equation (5.3). (See Appendix C)

The Gaussian and exponential basis functions are not orthogonal. In order to use an orthonormal set we employ the Gram-Schmidt orthonormalization procedure. This procedure is discussed in Appendix A.

The Laguerre basis functions are orthonormal and they have the following property:

$$\int_0^{\infty} g_i^L(r,b)g_j^L(r,b)dr = \delta_{ij} \tag{5.12}$$

The integrals involved in the matrix elements of $\tilde{H}$ can be computed analytically for the variational wave functions constructed from the Gaussian and exponential basis functions by utilizing [41].

$$\int_0^{\infty} r^{\alpha}e^{-a_i r^2}dr = \frac{\Gamma(\frac{\alpha+1}{2})}{a_i^{\frac{\alpha+1}{2}}} \tag{5.13}$$

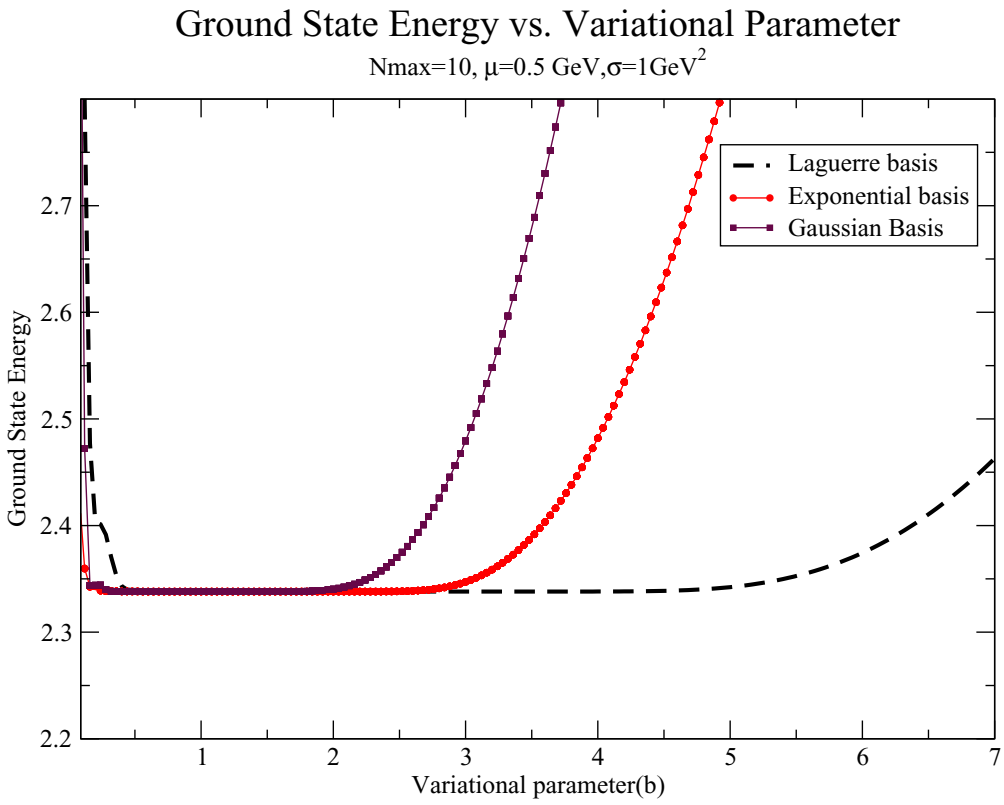

Figure 5.1: This is the plot of ground state energy vs. variational parameter for Gaussian, exponential and Laguerre basis functions. Note that the ground state energy stays constant over a the longest range of variational parameter for Laguerre basis functions.

and

$$\int_0^\infty r^\alpha e^{-a_i r} dr = \frac{\Gamma(\alpha+1)}{a_i^{\alpha+1}}. \tag{5.14}$$

The integrals involving the Laguerre variational wave functions are computed numerically via Gaussian quadrature [1]. Gaussian quadrature is discussed in Appendix B.

5.3 Test Case Results in Position-Space

We write a computer program to compute the discrete energies of the two-body system.[42]. To check the reliability of our computational scheme, we compute the energy states of the system with purely linear potential with unit linear strength ($\sigma = 1GeV^2$) and $m_1 = m_2 = 1GeV$ and $l = 0$.

Using this potential, equation (2.11) with $l = 0$ can be transformed into Airy's differential

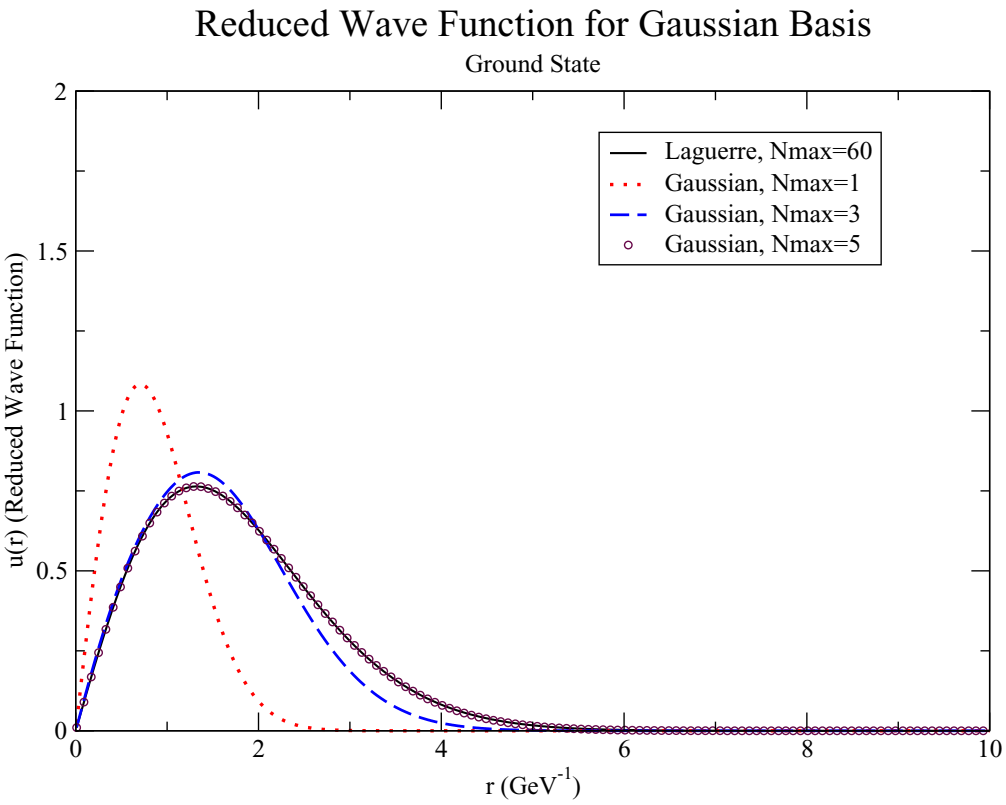

Figure 5.2: The normalized Gaussian variational wave functions for the ground state are plotted for number of basis $N_{\max} = 1, 3,$ and 5. The ground state Laguerre basis wave function with 60 basis is also plotted as a standard wavefunction. The Gaussian wave function converges to the Laguerre basis wave function(constructed with 60 basis functions) when $N_{\max}$ is increased from 3 to 5.

equation

$$\frac{d^2W}{dx^2} - xW = 0, \tag{5.15}$$

where the x is a transformed unitless variable:

$$x \equiv -\left(\frac{2\mu}{\sigma^2\hbar^2}\right)^{\frac{1}{3}}(E - \sigma r). \tag{5.16}$$

The normalizable solution to Airy's differential equation is the Airy's function:

$$W(x) = Ai(x). \tag{5.17}$$

The energies are related to the roots of the Airy's differential equation by the following relation:

$$E_{n-1} = \left(\frac{\sigma^2\hbar^2}{2\mu}\right)^{\frac{1}{3}}|x_n|, \tag{5.18}$$

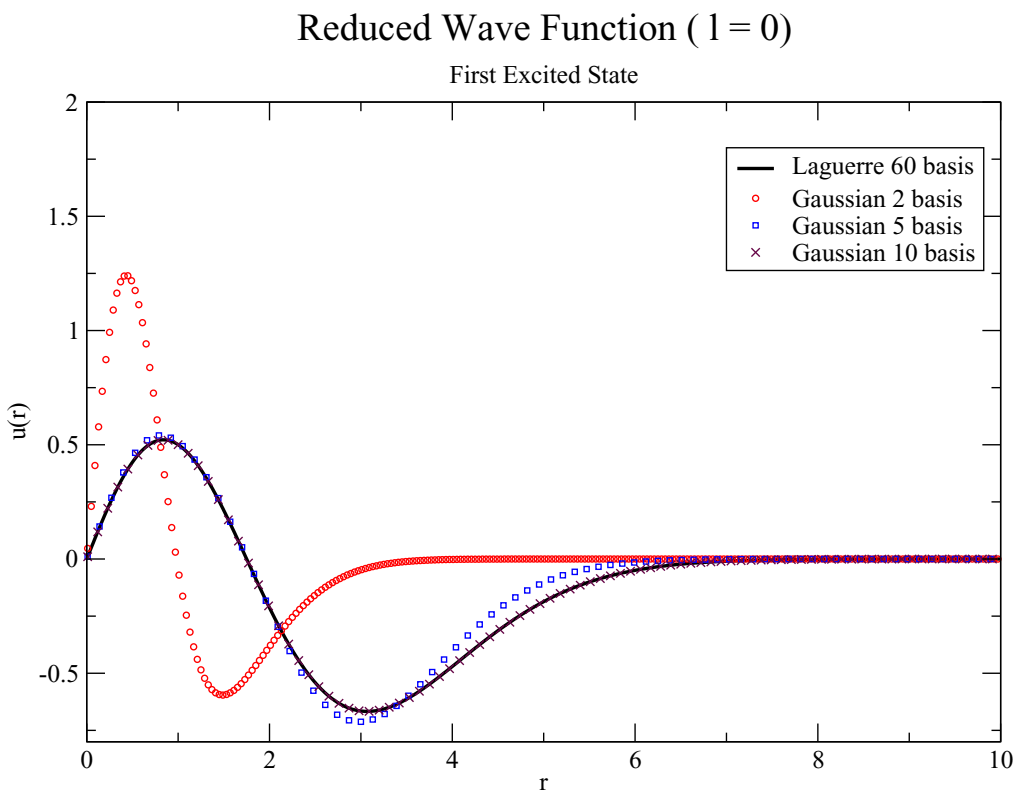

Figure 5.3: The normalized Gaussian variational wave functions for the first excited states are plotted for $N_{\max} = 2, 5$, and 10. The first excited state Laguerre basis wave function with 60 basis is also plotted as a standard wavefunction. Note that the wave function converges to the Laguerre basis wave function constructed from 60 basis functions when $N_{\max}$ is increased from 5 to 10.

where x_n are the roots of Airy's function. The results are given in Table (5.1). In figure 5.1, we have shown the plot of ground state energy as a function of variational parameter for Gaussian, exponential and Laguerre basis functions.

In figure 5.2, we have shown the plot of normalized ground state wave functions for number of basis $N_{\max} = 1, 3$, and 5. The ground state Laguerre basis wave function with 60 basis is also plotted as a standard wavefunction. The Gaussian wave function converges to the Laguerre basis wave function(constructed with 60 basis functions) when $N_{\max}$ is increased from 3 to 5.

In figure 5.3, we have shown the plot of normalized first excited state wave functions for number of basis $N_{\max} = 1, 3$, and 5. The first excited state Laguerre basis wave function with 60 basis is also plotted as a standard wavefunction. The Gaussian wave function converges to the Laguerre basis wave function(constructed with 60 basis functions) when $N_{\max}$ is increased from 3 to 5.

Table 5.1: S State ($l = 0$) Energies of the Gaussian, Exponential, and Laguerre Variational Wave Functions for $N_{\max} = 5$ and $N_{\max} = 10$. The Last Column Contains the Roots of the Airy's Function Given by Abramowitz and Stegun (A & S) [1]Results of The Laguerre basis with $N_{\max} = 60$ Agree to All Digits with A&S.

Basis function	$N_{\max} = 5$	$N_{\max} = 10$	A&S Laguerre $N_{max} = 60$
Gaussian			
1S	2.33812724	2.33810741	2.33810741
2S	4.11837280	4.08794945	4.08794944
3S	6.27318301	5.52055984	5.52055983
4S	11.37677573	6.78673566	6.78670809
5S	30.01762906	7.94767045	7.94413359
Exponential			
1S	2.33928309	2.33810944	2.33810741
2S	4.18895861	4.08827046	4.08794944
3S	5.86055714	5.52415263	5.52055983
4S	14.16858414	6.83240501	6.78670809
5S	75.58999149	8.34071492	7.94413359
Laguerre			
1S	2.34136432	2.33811592	2.33810741
2S	4.13333525	4.08857563	4.08794944
3S	5.72534717	5.53209461	5.52055983
4S	8.11423780	6.83859440	6.78670809
5S	15.51904879	8.14892461	7.94413359

5.4 Solution in Momentum-Space

We will solve equation (3.7) by expanding the wave function in a complete set of basis functions. Since equation(3.7) has momentum-space wavefunction, we'll expand the wavefunction as a linear combination of the momentum-space basis.
We expand the wavefunctions as

$$\phi_{nl}(p) = \sum_{j=0}^{\infty} g_j(p) c_j \tag{5.19}$$

where $g_j(p)$ are known functions(See Appendix C).
The Jacobi basis functions in momentum-space are given as

$$g_j(p) = \frac{1}{\sqrt{N_{jl}}} \frac{(p/b)^l}{[(p/b)^2+1]^{l+2}} P_j^{(l+\frac{3}{2},l+\frac{1}{2})} \left[\frac{p^2-b^2}{p^2+b^2}\right], \tag{5.20}$$

where $P_j^{\alpha,\beta}(p/b)$ are the Jacobi polynomials and N_{jl} is

$$N_{jl} = \frac{b^3}{2(2j+2l+3)} \frac{\Gamma(j+l+\frac{5}{2})\Gamma(j+l+\frac{3}{2})}{j!\Gamma(j+2l+3)} \tag{5.21}$$

Using above expansion given in equation(5.19), we get

$$\sum_{j=0}^{\infty} \frac{\mathbf{p}^2}{2\mu} g_j(p)c_j + \sum_{j=0}^{\infty} \int_0^{\infty} V_l(p,p')g_j(p')p'^2 dp' c_j = E \sum_{j=0}^{\infty} g_j(p)c_j$$

Next we multiply through by $p^2 g_i(p)$ and integrate over the momentum and we get

$$\begin{aligned} &\sum_{j=0}^{\infty} c_j \left[\int_0^{\infty} \frac{\mathbf{p}^2}{2\mu} g_i(p)g_j(p)p^2 dp \right] \\ + &\sum_{j=0}^{\infty} c_j \left[\int_0^{\infty} \int_0^{\infty} V_l(p,p')g_i(p)g_j(p')p'^2 dp' p^2 dp \right] c_j = E \sum_{j=0}^{\infty} c_j \left[g_i(p)g_j(p)p^2 dp \right] \end{aligned} \tag{5.22}$$

This is a simple eigen equation and can be solved by standard method.

5.5 Test Case Results in Momentum-Space

To check the reliability of our computational scheme, we compute the energy states of the system with pure linear potential with unit linear strength($\sigma = 1GeV^2$) and $m_1 = m_2 = 1GeV$ and $l = 0$. We used these parameters because analytical results are available as the roots of Airy's function.

As we have noticed in the previous section that with the above mentioned parameters, the two-body Schrödinger equation becomes equivalent to the Airy's differential equation and the energies are related to the roots of the Airy's differential equation. The results are given in Table(5.2)

5.6 Solution in Mixed Space

Now we will solve the mixed space equation (4.7) by expanding the wave function in a complete set of basis functions. Since equation (4.7) has both the momentum-space and position-space wave functions, we expand both in a complete set of basis functions which are Fourier-Bessel transforms of one another. Two well known sets are the Laguerre/Jacboi [43] and the harmonic oscillator basis [43].
We expand the wavefunctions as

$$\psi_{nl}(r) = \sum_{j=0}^{\infty} g_j(r)c_j \tag{5.23}$$

$$\phi_{nl}(p) = \sum_{j=0}^{\infty} \tilde{g}_j(p)c_j \tag{5.24}$$

Table 5.2: S State ($l = 0$) Energies of the Gaussian, Harmonic Oscillator and Jacobi Variational Wave Functions for $N_{\max} = 10$ and $N_{\max} = 20$. The Last Column Contains the Roots of the Airy's Function Given by Abramowitz and Stegun (A & S) [1].

Basis	$N_{\max} = 10$	$N_{\max} = 20$	A&S
Gaussian			
1S	2.33810815	2.33810750	2.33810741
2S	4.08795437	4.08794955	4.08794944
3S	5.52085236	5.52056003	5.52055983
4S	6.79481014	6.78671124	6.78670809
5S	8.00139967	7.94424647	7.94413359
H.O.			
1S	2.33811101	2.33810749	2.33810741
2S	4.08899547	4.08794955	4.08794944
3S	5.56607385	5.52057865	5.52055983
4S	7.16626004	6.78810139	6.78670809
5S	9.24612681	7.97280314	7.94413359
Jacobi			
1S	2.33811592	2.33810741	2.33810741
2S	4.08857562	4.08794946	4.08794944
3S	5.53209460	5.52056175	5.52055983
4S	6.83859440	6.78678502	6.78670809
5S	8.14892460	7.94526089	7.94413359

We note that the basis functions are related by the Fourier-Bessel transform

$$\tilde{g}_i(p) = \sqrt{\tfrac{2}{\pi}} \int_0^\infty j_l(pr) g_i(r) r^2 dr \tag{5.25}$$

$$g_i(r) = \sqrt{\tfrac{2}{\pi}} \int_0^\infty j_l(pr) \tilde{g}_i(p) p^2 dp \tag{5.26}$$

If we use the expansion in equation (4.7), we obtain

$$\sum_{j=0}^{\infty} \frac{\mathbf{p}^2}{2\mu} \tilde{g}_j(p) c_j \tag{5.27}$$

$$+ \sum_{j=0}^{\infty} \sqrt{\frac{2}{\pi}} \int_0^\infty j_l(pr) V(r) g_j(r) r^2 dr c_j = E \sum_{j=0}^{\infty} \tilde{g}_j(p) c_j$$

Next we multiply through by $p^2\tilde{g}_i(p)$ and integrate over the momentum

$$\sum_{j=0}^{\infty} c_j \int_0^{\infty} \frac{\mathbf{p}^2}{2\mu} \tilde{g}_i(p)\tilde{g}_j(p)p^2dp \tag{5.28}$$

$$+ \quad \sum_{j=0}^{\infty} c_j \sqrt{\frac{2}{\pi}} \int_0^{\infty}\int_0^{\infty} j_l(pr)V(r)\tilde{g}_i(p)g_j(r)p^2r^2drdp = E\sum_{j=0}^{\infty} c_j \int_0^{\infty} \tilde{g}_i(p)g_j(p)p^2dp \tag{5.29}$$

Using the equation(5.26) on the above equation and because of the orthonormality of the basis functions we obtain the following:

$$\sum_{j=0}^{\infty} c_j \int_0^{\infty} \frac{\mathbf{p}^2}{2\mu} \tilde{g}_i(p)\tilde{g}_j(p)p^2dp \tag{5.30}$$

$$+ \quad \sum_{j=0}^{\infty} c_j \int_0^{\infty} V(r)g_i(r)g_j(r)r^2dr = Ec_i$$

This is a simple matrix eigen-equation and can be solved by standard methods.

5.7 Test Case Results in Mixed-Space

To check the reliability of our mixed-space computational scheme, we compute the energy states of the system with pure linear potential with unit linear strength($\sigma = 1GeV^2$) and $m_1 = m_2 = 1GeV$ and $l = 0$. As we have noticed in earlier part that with the above mentioned parameters, the two-body Schrödinger equation becomes equivalent to the Airy's differential equation and the energies are related to the roots of the Airy's differential equation. The results are given in Table(5.3)

Table 5.3: S State ($l = 0$) Energies of the Gaussian, Harmonic Oscillator and Laguerre/Jacobi Variational Wave Functions for $N_{\max} = 10$ and $N_{\max} = 20$. The Last Column Contains the Roots of the Airy's Function Given by Abramowitz and Stegun (A & S) [1]

Basis	$N_{\max} = 10$	$N_{\max} = 20$	A&S
Gaussian			
1S	2.34572367	2.33810331	2.33810741
2S	4.10596083	4.10308625	4.08794944
3S	6.06540293	5.64423865	5.52055983
4S	10.76819625	6.98916741	6.78670809
5S	19.35362119	10.08586765	7.94413359
H.O.			
1S	2.33811102	2.33810749	2.33810741
2S	4.08899547	4.08794955	4.08794944
3S	5.56607368	5.52057876	5.52055983
4S	7.16625905	6.78811037	6.78670809
5S	9.24612427	7.97293645	7.94413359
Laguerre/Jacobi			
1S	2.33811592	2.33810741	2.33810741
2S	4.08857563	4.08794947	4.08794944
3S	5.53209461	5.52056175	5.52055983
4S	6.83859440	6.78678503	6.78670809
5S	8.14892461	7.94526090	7.94413359

Chapter 6

SPINLESS SALPETER EQUATION IN MIXED REPRESENTATION

6.1 Spinless Salpeter Equation

The spinless Salpeter equation is obtained by replacing the Schrödinger kinetic energy operator by the relativistic kinetic energy T [44][45]. For the one body equation, the replacement is $T = \sqrt{p^2 + m^2}$, where $p \equiv |\mathbf{p}|$ is the 3-momentum of the particle and m is the mass. For the two body equation, the replacement is $T = T_1 + T_2 = \sqrt{p^2 + m_1^2} + \sqrt{p^2 + m_2^2}$, with $\mathbf{p} = \mathbf{p}_1 = -\mathbf{p}_2$. By doing this replacement, E now contains the rest masses m_1 and m_2.

6.2 Spinless Salpeter Equation in Mixed-Space

A short derivation of the spinless Salpeter equation in the mixed representation is now presented. In Hilbert space

$$(\hat{T} + \hat{V})|\Psi\rangle = E|\Psi\rangle, \tag{6.1}$$

where $|\Psi\rangle$ is the wave vector, $\hat{T} \equiv \sqrt{p^2 + m_1^2} + \sqrt{p^2 + m_2^2}$ and $\hat{V}$ is the operator for the potential. E is the total energy.

After projecting with $\langle \mathbf{p}|$ from the left and inserting momentum space completeness, position space completeness and using the definition of a local potential, i.e. $\langle \mathbf{r}|\hat{V}|\mathbf{r}'\rangle = V(r)\delta(\mathbf{r} - \mathbf{r}')$, we obtain

$$\begin{aligned} & \left(\sqrt{\mathbf{p}^2 + m_1^2} + \sqrt{\mathbf{p}^2 + m_2^2}\right)\Phi(\mathbf{p}) \\ + \quad & \frac{1}{(2\pi)^{3/2}} \int e^{-i\mathbf{p}\cdot\mathbf{r}} V(r)\Psi(\mathbf{r}) d\mathbf{r} = E\Phi(\mathbf{p}). \end{aligned} \tag{6.2}$$

This is the 3-dimensional spinless Salpeter equation in the mixed-space representation. $\Phi(\mathbf{p})$ is the Fourier transform of the position space wave function $\Psi(\mathbf{r})$ and is given by

$$\Phi(\mathbf{p}) = \frac{1}{(2\pi)^{3/2}} \int e^{-i\mathbf{p}\cdot\mathbf{r}} \Psi(\mathbf{r}) d\mathbf{r}. \tag{6.3}$$

When there is no coupling between angular momenta, then $\Psi(\mathbf{r}) = \psi_{nl}(r) Y_l^m(\hat{r})$ and $\Phi(\mathbf{p}) = \phi_{nl}(p) Y_l^m(\hat{p})$. Using this angular separation, expanding the plane wave and performing the angular integration, we obtain

$$\left(\sqrt{p^2+m_1^2}+\sqrt{p^2+m_2^2}\right)\phi_{nl}(p)$$
$$+\quad\sqrt{\frac{2}{\pi}}\int_0^\infty j_l(pr)V(r)\psi_{nl}(r)r^2dr = E\phi_{nl}(p), \tag{6.4}$$

where $j_l(pr)$ is the spherical Bessel function of order l. The position space and momentum space wave functions are related by a Fourier-Bessel transform

$$\phi_{nl}(p) = \sqrt{\tfrac{2}{\pi}}\int_0^\infty j_l(pr)\psi_{nl}(r)r^2dr, \tag{6.5}$$
$$\psi_{nl}(r) = \sqrt{\tfrac{2}{\pi}}\int_0^\infty j_l(pr)\phi_{nl}(p)p^2dp, \tag{6.6}$$

In the last two equations a factor of $(-i)^l$ is absorbed into the definition of $\psi_{nl}(r)$.

Equation (6.4) is the spinless Salpeter equation for the l partial wave in the mixed space representation. It is solved by expanding the wave functions in a complete set of basis functions. Since equation (6.4) has both the momentum space and position space wave functions, we expand both in a complete set of basis functions which are Fourier-Bessel transforms of one another. Two well-known sets are the Laguerre-Jacobi and the harmonic oscillator basis. We expand the wavefunctions as

$$\psi_{nl}(r) = \sum_{j=0}^\infty g_j(r)c_j, \tag{6.7}$$
$$\phi_{nl}(p) = \sum_{j=0}^\infty \tilde{g}_j(p)c_j. \tag{6.8}$$

Here $g_j(r)$ and $\tilde{g}_j(p)$ are the basis functions described in Appendix C. The c_j terms are the expansion coefficients.We note that the basis functions are related by the Fourier-Bessel transform

$$\tilde{g}_i(p) = \sqrt{\tfrac{2}{\pi}}\int_0^\infty j_l(pr)g_i(r)r^2dr \tag{6.9}$$
$$g_i(r) = \sqrt{\tfrac{2}{\pi}}\int_0^\infty j_l(pr)\tilde{g}_i(p)p^2dp. \tag{6.10}$$

In the variational method, one expands the wave function in a complete orthonormal set of basis functions as in equations. One minimizes the energy by varying the coefficients of the expansion. This results in a matrix eigen-equation. If one uses a complete set of basis, the matrix is an infinite dimensional matrix. Solving the matrix eigen-equation is equivalent to minimizing the energy with respect to the coefficients. In practice, one cannot use an infinite set of basis functions and therefore must use a finite set of basis functions. To compensate

for this truncation, we introduce a parameter in the basis functions which can be used as a variational parameter.

Using the above expansion in equation (6.4) gives

$$\begin{aligned} & \sum_{j=0}^{\infty}\left(\sqrt{p^2+m_1^2}+\sqrt{p^2+m_2^2}\right)\tilde{g}_j(p)c_j \\ + & \sum_{j=0}^{\infty}\sqrt{\frac{2}{\pi}}\int_0^{\infty} j_l(pr)V(r)g_j(r)r^2drc_j = E\sum_{j=0}^{\infty}\tilde{g}_j(p)c_j. \end{aligned} \tag{6.11}$$

Next, multiply through by $p^2\tilde{g}_i(p)$ and integrate over the momentum,

$$\begin{aligned} & \sum_{j=0}^{\infty}c_j\int_0^{\infty}\left(\sqrt{p^2+m_1^2}+\sqrt{p^2+m_2^2}\right)\tilde{g}_i(p)\tilde{g}_j(p)p^2dp \\ + & \sum_{j=0}^{\infty}c_j\sqrt{\frac{2}{\pi}}\int_0^{\infty}\int_0^{\infty} j_l(pr)V(r)\tilde{g}_i(p)g_j(r)p^2r^2drdp \\ & = E\sum_{j=0}^{\infty}c_j\int_0^{\infty}\tilde{g}_i(p)g_j(p)p^2dp. \end{aligned} \tag{6.12}$$

Using the relation given in equation (6.10) on the second term of the above equation and because of the orthonormality of the basis functions, we obtain

$$\begin{aligned} & \sum_{j=0}^{\infty}c_j\int_0^{\infty}\left(\sqrt{p^2+m_1^2}+\sqrt{p^2+m_2^2}\right)\tilde{g}_i(p)\tilde{g}_j(p)p^2dp \\ + & \sum_{j=0}^{\infty}c_j\int_0^{\infty}V(r)g_i(r)g_j(r)r^2dr = Ec_i. \end{aligned} \tag{6.13}$$

This can be written as

$$\sum_{j=0}^{\infty}H_{ij}c_j = Ec_i, \tag{6.14}$$

where

$$\begin{aligned} H_{ij} = & \int_0^{\infty}\left(\sqrt{p^2+m_1^2}+\sqrt{p^2+m_2^2}\right)\tilde{g}_i(p)\tilde{g}_j(p)p^2dp \\ & + \int_0^{\infty}V(r)g_i(r)g_j(r)r^2dr. \end{aligned} \tag{6.15}$$

Equation (6.14) is a simple matrix eigenvalue equation that can be solved by standard methods.

6.3 Results

The spinless Salpeter equation in mixed space has been solved using the variational principle. Both the mixed space and momentum space spinless Salpeter equations were solved in order to confirm the results of the momentum space calculations with the mixed space results.

Before discussing the results, we discuss briefly to explain how experimental spin average values are calculated. Each quark has spin 1/2. When two quarks are involved, one obtains a total spin S = 0 or S = 1. For $l = 0$ (S state), one has the S = 0 state(singlet) and S=1 state(triplet). In spectroscopic notation of $n^{2s+1}L_J$ we can express these states as n^1S_0 and n^3S_1. Here J is the total angular momentum and L is the orbital angular momentum. The spin averaged mass $m_{\rm av}^{l=0}$(S state) is calculated as

$$m_{\rm av}^{l=0} \equiv (m_{n^1S_0} + 3m_{n^3S_1})/4. \tag{6.16}$$

For $l = 1$ (P state), one has the S = 0 state(singlet) and S=1 state(triplet). In spectroscopic notation of $n^{2s+1}L_J$ we can express these states as n^1P_1,n^3P_2,n^3P_1 and n^3P_0. The spin averaged mass $m_{\rm av}^{l=1}$ is calculated as

$$m_{\rm av}^{l=1} \equiv (3m_{n^1P_1} + 1m_{n^3P_0} + 3m_{n^3P_1} + 5m_{n^3P_2})/12. \tag{6.17}$$

For $l = 2$ (D state), one has the S = 0 state(singlet) and S=1 state(triplet). In spectroscopic notation of $n^{2s+1}L_J$ we can express these states as n^1D_2,n^3D_2,n^3D_1 and n^3D_3. The spin averaged mass $m_{\rm av}^{l=2}$ is calculated as

$$m_{\rm av}^{l=2} \equiv (5m_{n^1D_2} + 5m_{n^3D_2} + 3m_{n^3D_1} + 7m_{n^3D_3})/20. \tag{6.18}$$

The following Table(6.1) contains the parameters used in our computation. The Table(6.2) and Table(6.3) contain the results for the spin-averaged meson masses obtained by mixed-space and momentum-space spinless Salpeter equation.

Table 6.1: Parameters Used for the Mixed-Space and Momentum-Space Equations.

Parameter	Mixed space	Momentum space
σ (GeV^2)	0.197	0.197
C	-0.5	-0.5
m_c(GeV)	1.35475	1.35475
m_b (GeV)	4.7721	4.7721

Table 6.2: Calculations of $c\bar{c}$ Spin-Averaged Masses with the Mixed-Space and Momentum-Space Equations Compared to Experiment[2]. The States Marked with † are a Mixture of S and D States, but have been Assigned as Predominantly S or D Based on the Analysis of Reference [3]. The States with the Error Bars have been Spin-Averaged. We Fit to the $1S$ and $2S$ States within the Tolerance $\varepsilon \leq 0.0002$.

State	Mixed space	Momentum space	Experiment
$1S$	3067.71	3067.71	3067.76 ± 0.31
$2S$	3673.84	3673.84	3673.82 ± 1.03
$3S$	4113.95	4113.95	$4039^{\dagger}$
$4S$	4483.13	4483.13	$4421^{\dagger}$
$5S$	4809.60	4809.60	
$6S$	5106.43	5106.43	
$1P$	3522.68	3522.68	3525.46 ± 0.15
$2P$	3982.45	3982.45	
$3P$	4364.49	4364.49	
$4P$	4700.32	4700.32	
$5P$	5004.40	5004.40	
$6P$	5284.84	5284.84	
$1D$	3829.37	3829.37	3773
$2D$	4227.25	4227.25	$4153^{\dagger}$
$3D$	4574.38	4574.38	
$4D$	4887.11	4887.11	
$5D$	5174.48	5174.48	
$6D$	5442.09	5442.09	

Table 6.3: Calculations of $b\bar{b}$ Spin-Averaged Masses with the Mixed-Space and Momentum-Space Equations Compared to Experiment[2]. The States Marked with † are a Mixture of S and D States, but have been Assigned as Predominantly S or D Based on the Analysis of Reference [3]. The States with the Error Bars have been Spin-Averaged. We Fit to the $1S$ State within the Tolerance $\varepsilon \leq 0.0002$.

State	Mixed space	Momentum space	Experiment
$1S$	9420.21	9420.21	9420.22 ± 7.2
$2S$	10015.82	10015.82	10023
$3S$	10373.57	10373.57	10355
$4S$	10661.68	10661.68	10579
$5S$	10913.24	10913.24	$10865^{\dagger}$
$6S$	11141.18	11141.18	$11019^{\dagger}$
$1P$	9929.15	9929.15	9900
$2P$	10293.90	10293.90	10260
$3P$	10587.28	10587.28	
$4P$	10842.92	10842.92	
$5P$	11074.15	11074.15	
$6P$	11287.82	11287.82	
$1D$	10186.83	10186.83	
$2D$	10490.27	10490.27	
$3D$	10752.94	10752.94	
$4D$	10989.50	10989.50	
$5D$	11207.43	11207.43	
$6D$	11411.16	11411.16	

Chapter 7

EMPLOYING SPIN-DEPENDENT INTERACTIONS

7.1 Spin-Dependent Potentials

According to the quark model, each meson is a two-body bound-state of a quark and an antiquark. Like any quantum mechanical system, the quark-antiquark($q\bar{q}$) pair has a discrete energy level spectrum corresponding to the different modes of $q\bar{q}$ excitations, rotations, vibrations and so on.[5] These discrete energies must correspond to the observed meson states. Even in the absence of knowledge about the potential which binds the quark to the antiquark, the model is very predictive. Each quark has spin $\frac{1}{2}$, so the total intrinsic spin of the $q\bar{q}$ pair can be either $S = 0$ or 1. The spin J of the composite meson is the vector sum of this spin S and the relative orbital angular momentum L of the q and $\bar{q}$.

The spin-dependent potential we used is given by

$$V_{sd}(r) = V_{LS}(r)\mathbf{L}.\mathbf{S} + \frac{8C}{3\mu^2\sqrt{\pi}}V_{SS}(r)\mathbf{S_1}.\mathbf{S_2} + A \tag{7.1}$$

where $\mathbf{L}.\mathbf{S}|\Psi\rangle = [\frac{j(j+1)-l(l+1)-s(s+1)}{2}]|\Psi\rangle$
and $V_{LS}(r) = \left[\frac{\sigma}{r} + V_{LS_1}e^{-\beta r^2}\right]$
and $\mathbf{S_1}.\mathbf{S_2}|\Psi\rangle = \left[\frac{s(s+1)}{2} - \frac{3}{4}\right]|\Psi\rangle$
and $V_{SS}(r) = k^3\mu^3 e^{-k^2\mu^2 r^2}$
A is an additive constant.

The first term is for the spin-orbit interaction and the second term is for the spin-spin interaction and the last term is a constant. The spin-spin potential was approximated using a smeared delta function, $e^{-k^2\mu^2 r^2}$.
The conventional spin-orbit potential [46] [9] [47] [48] [49] is proportional to

$$\frac{1}{r}\frac{dV}{dr} = \frac{\sigma}{r} + \frac{C}{r^3} \tag{7.2}$$

The $\frac{C}{r^3}$ term is too singular and can only be treated perturbatively. Therefore, we approximated the $\frac{C}{r^3}$ part of the spin-orbit potential by using a Gaussian function $V_{LS_1}e^{-\beta r^2}$. The parameter β is used to simulate the behavior of the $\frac{1}{r^3}$ term, whereas the constant V_{LS_1} is the cutoff depth of the spin-orbit potential.

7.2 Spin-Orbit Coupling

Spin-orbit coupling comes from the interaction between the orbital angular momentum(**L**) and spin(**S**) of the system. Since total angular momentum (**J**) is defined as the vector sum of **L** and **S**, we can write

$$\mathbf{J}^2 = \mathbf{L}^2 + \mathbf{S}^2 + 2\mathbf{L}\cdot\mathbf{S} \tag{7.3}$$

So, the dot product **L**.**S** can be expressed as

$$\mathbf{L}\cdot\mathbf{S} = \frac{1}{2}(\mathbf{J}^2 - \mathbf{L}^2 - \mathbf{S}^2) \tag{7.4}$$

Since $\mathbf{J}^2$, $\mathbf{L}^2$ and $\mathbf{S}^2$ are all eigen operators which commute with the Hamiltonian H, and we know that

$$\mathbf{J}^2|\Psi\rangle = j(j+1)|\Psi\rangle \tag{7.5}$$

and

$$\mathbf{L}^2|\Psi\rangle = l(l+1)|\Psi\rangle \tag{7.6}$$

and

$$\mathbf{S}^2|\Psi\rangle = s(s+1)|\Psi\rangle \tag{7.7}$$

where j, l, s are scalars. We therefore obtain

$$\mathbf{L}.\mathbf{S}|\Psi\rangle = \frac{1}{2}[j(j+1) - l(l+1) - s(s+1)]|\Psi\rangle \tag{7.8}$$

In a system of one quark and one antiquark, the total spin(s) is always 0(singlet) or 1(triplet). In the triplet case we can have $j = l$(when s is 0) or $j \to l+1, l-1$.
The spin-orbit part of the potential is then

$$V_{LS}(r)\mathbf{L}.\mathbf{S} \to \frac{1}{2}[j(j+1) - l(l+1) - s(s+1)]\left[\frac{\sigma}{r} + V_{LS_1}e^{-\beta r^2}\right] \tag{7.9}$$

This form of the potential has been used in our model to compute the fine splitting of the meson mass spectra.

7.3 Spin-Spin Interaction

Spin-spin interaction is the cause behind the hyperfine splitting. In spin-spin interaction, the spin of each particle interact on one another. Spin-spin interaction is expressed as:

$$V_{SS}(r)\mathbf{S_1}.\mathbf{S_2} \tag{7.10}$$

$\mathbf{S_1}.\mathbf{S_2}$ can be written as the following:

$$\mathbf{S_1}.\mathbf{S_2} = \frac{\mathbf{S}^2}{2} - \frac{3}{4} \tag{7.11}$$

where **S**=total spin of two particles.

For singlet states, when $s = 0$, the contribution of the spin-spin interaction is $-\frac{3}{4}$. For triplet states, when $s = 1$, the contribution of the spin-spin interaction is $\frac{1}{4}$. Note that for each l, this spin-spin interaction gives the hyperfine splitting in the meson mass spectra.

The spin-spin part of the potential is taken to be:

$$\frac{8C}{3\mu^2\sqrt{\pi}}(\mathbf{S_1}.\mathbf{S_2})k^3\mu^3 e^{-k^2\mu^2 r^2} \tag{7.12}$$

The spin-spin potential was approximated using a smeared delta function, $e^{-k^2\mu^2 r^2}$. Other researchers also used similar type of smeared delta functions to handle spin-spin interactions[50].

Chapter 8

MESON MASS SPECTROSCOPY

Meson mass spectroscopy plays a very important role in fundamental particle physics. Studying meson mass spectra gives us the insight and the knowledge about the nature and dynamics of strong interaction between the quarks. It also helps us to understand the nature of the constituent glue, the exchange particle between quarks, known as gluons.

It is important that our theoretical description of the quark-antiquark system should be very accurate and consistent. However, gluons carry color charge. Since they carry color charge, gluons interact with one another. The strong self-interaction between gluons gives rise to such complex non-linear equations that the detailed and accurate theoretical description of the $q\bar{q}$ system becomes extremely difficult.

Lattice gauge calculations partially solved the problem. Lattice gauge calculations indicates that in the static quark limit, a linearly rising confining potential and a Coulomb-type potential can very well describe the true potential between quarks. Linearly rising potential handles the property of confinement. Due to asymptotic freedom, one gluon exchange takes place between quarks when they are very close to each other. One gluon exchange gives rise to the Coulomb-type interaction [14].

8.1 Heavy-Heavy Systems

The models with a linearly rising and a Coulomb-type potential successfully describes the mesonic system containing one heavy quark and one heavy antiquark [16]. We have included the relativistic kinematics along with the linear, Coulomb-type and the spin-dependent potentials in our computations. The two-body equation we used is known as mixed-space Salpeter equation.

The potential we used for the mixed-space Salpeter equation is given by

$$V(r) = \sigma r - C/r + V_{LS}(r)\mathbf{L}.\mathbf{S} + \frac{8C}{3\mu^2\sqrt{\pi}}V_{SS}(r)\mathbf{S_1}.\mathbf{S_2} + A \tag{8.1}$$

where $V_{LS}(r) = \left[\frac{\sigma}{r} + V_{LS_1}e^{-\beta r^2}\right]$

and $V_{SS}(r) = k^3\mu^3 e^{-k^2\mu^2 r^2}$

A is an additive constant.

In equation(8.1), the first term is the linear confining term, the second term is for the Coulomb-type interaction, the third term is for the spin-orbit interaction and the fourth term is for the

spin-spin interaction and the last term is a constant. The spin-spin potential was approximated using a smeared delta function, $e^{-k^2\mu^2 r^2}$.

The conventional spin-orbit potential is proportional to

$$\frac{1}{r}\frac{dV}{dr} = \frac{\sigma}{r} + \frac{C}{r^3} \tag{8.2}$$

The $\frac{C}{r^3}$ term is too singular and can only be treated perturbatively. Therefore, we approximated the $\frac{C}{r^3}$ part of the spin-orbit potential by using a Gaussian function $V_{LS_1}e^{-\beta r^2}$. The parameter β is used to simulate the behavior of the $\frac{1}{r^3}$ term, whereas the constant V_{LS_1} is the cutoff depth of the spin- orbit potential.

The following tables contains the mass spectra of $c\bar{c}$ and $b\bar{b}$ mesonic systems. These are mesons made of two equal mass heavy quarks.

We fit to the experimentally available data for the singlet (1^1S_0) and triplet(1^3S_1) states of $c\bar{c}$ and obtain the values of the linear coupling constant σ, the Coulomb constant C and the constituent mass of the charm quark. From the energy gap of singlet and triplet states, we obtain the the spin-spin interaction parameter, k. Then we fit to the experimentally available triplet states for P($l = 1$) states for $j = 0, 1, 2$, the states are ($1^3P_0, 1^3P_1, 1^3P_2$). From the energy gap, we obtain the values of the parameters V_{LS_1}(cutoff depth) and β.

We repeat the same procedure for $b\bar{b}$ spectra. We use the same linear coupling constant σ and Coulomb constant C for $b\bar{b}$. Obviously the constituent mass used for bottom quark is different since mass of bottom quark is about four times than that of charm quark. Then we find the spin-spin parameter and spin-orbit parameters by fitting to the energy gap of singlet and triplet states.

The results for the higher excited states produced by our calculations are the predicted theoretical values. We have shown the percent error of these predicted values compared to the experimental values (in the cases where experimental values are available).

For the heavy-heavy systems, no additive constant is required. To produce the $b\bar{b}$ and $c\bar{c}$ spectra, we use additive constant $A = 0$ in our calculations.

All experimental data are taken from the particle data group's latest meson summary table[2].

Table 8.1: $c\bar{c}$ Meson System, $m_c = 1.361$ GeV, Linear Strength = $\sigma = 0.191\ GeV^2$, Coulomb Strength=0.5, Spin-Spin Interaction Parameter= $k = 0.771$, Spin-Orbit Parameters: $\beta = 1.573 GeV^2$ and $V_{LS_1} = 0.0129$ GeV. Experimental Values are taken from the Current Available Particle Data[2].

State	Meson	Exp. Val (MeV)	Uncertainty (MeV)	Mixed-Space Calculation (MeV)	Per Error (%)
1^1S_0	$\eta_c(1S)$	2980.5	1.2	2979.91	0.02
2^1S_0	$\eta_c(2S)$	3637	4	3628.99	0.22
3^1S_0				4070.26	
4^1S_0				4437.04	
5^1S_0				4760.16	
6^1S_0				5053.36	
1^3S_1	$J/\Psi(1S)$	3096.916	0.011	3096.06	0.03
2^3S_1	$\Psi(2S)$	3686.09	0.04	3675.42	0.29
3^3S_1	$\Psi(4040)$	4039	1	4104.16	1.61
4^3S_1	$\Psi(4415)$	4421	4	4464.89	0.99
5^3S_1				4784.32	
6^3S_1				5074.99	
1^3P_0	$\chi_{c0}(1P)$	3414.75	0.31	3369.09	1.34
2^3P_0				3846.17	
3^3P_0				4235.29	
4^3P_0				4574.22	
5^3P_0				4879.43	
6^3P_0				5159.91	
1^3P_1	$\chi_{c1}(1P)$	3510.66	0.07	3449.78	1.73
2^3P_1				3911.95	
3^3P_1				4292.91	
4^3P_1				4626.51	
5^3P_1				4927.89	
6^3P_1				5205.44	

Table 8.2: $c\bar{c}$ Meson System (Continued)

State	Meson	Exp. Val (MeV)	Uncertainty (MeV)	Mixed-Space Calculation (MeV)	Per Error (%)
1^3P_2	$\chi_{c2}(1P)$	3556.20	0.09	3598.22	1.18
2^3P_2	$\chi_{c2}(2P)$	3929	5	4034.88	2.69
3^3P_2				4401.48	
4^3P_2				4725.55	
5^3P_2				5020.01	
6^3P_2				5292.21	
1^1P_1	h_c	3525.67	0.32	3482.49	1.22
2^1P_1				3942.60	
3^1P_1				4321.74	
4^1P_1				4653.81	
5^1P_1				4953.95	
6^1P_1				5230.48	
1^3D_1	$\Psi(3770)$	3772.92	0.35	3651.45	3.22
2^3D_1	$\Psi(4160)$	4153	3	4062.95	2.17
3^3D_1				4416.73	
4^3D_1				4732.95	
5^3D_1				5022.06	
6^3D_1				5290.38	

Table 8.3: $b\bar{b}$ Meson System, $m_b = 4.787$ GeV, Linear Strength = $\sigma = 0.191\ GeV^2$, Coulomb Strength=0.5, Spin-Spin Interaction Parameter= $k = 0.4315$, Spin-Orbit Parameters: $\beta = 2.73 GeV^2$ and $V_{LS_1} = 0.15$ GeV. Experimental Values are Taken from the Current Available Particle Data[2].

State	Meson	Exp. Val (MeV)	Uncertainty (MeV)	Mixed-Space Calculation (MeV)	Per Error (%)
1^1S_0	$\eta_b(1S)$	9388.9	4.0/-3.5	9388.76	0.00
2^1S_0				10017.51	
3^1S_0				10373.48	
4^1S_0				10658.04	
5^1S_0				10905.81	
6^1S_0				11130.00	
1^3S_1	$\Upsilon(1S)$	9460.30	0.26	9460.80	0.01
2^3S_1	$\Upsilon(2S)$	10,023.26	0.31	10035.98	0.13
3^3S_1	$\Upsilon(3S)$	10,355.2	0.5	10385.82	0.30
4^3S_1	$\Upsilon(4S)$	10,579.4	1.2	10667.83	0.84
5^3S_1	$\Upsilon(10860)$	10,865	8	10914.14	0.45
6^3S_1	$\Upsilon(11020)$	11,019	8	11137.35	1.07
1^3P_0	$\chi_{b0}(1P)$	9859.44	0.73	9658.88	2.03
2^3P_0	$\chi_{b0}(2P)$	10,232.5	0.9	10098.80	1.31
3^3P_0				10423.53	
4^3P_0				10696.03	
5^3P_0				10937.50	
6^3P_0				11157.79	
1^3P_1	$\chi_{b1}(1P)$	9892.78	0.57	9815.82	0.78
2^3P_1	$\chi_{b1}(2P)$	10,254.6	0.72	10208.36	0.46
3^3P_1				10512.35	
4^3P_1				10772.84	
5^3P_1				11006.28	
6^3P_1				11220.75	

Table 8.4: $b\bar{b}$ Meson System (Continued)

State	Meson	Exp. Val (MeV)	Uncertainty (MeV)	Mixed-Space Calculation (MeV)	Per Error (%)
1^3P_2	$\chi_{b2}(1P)$	9912.21	0.57	10069.79	1.59
2^3P_2	$\chi_{b2}(2P)$	10,268.65	0.72	10399.24	1.27
3^3P_2				10672.51	
4^3P_2				10914.04	
5^3P_2				11134.28	
6^3P_2				11338.87	
1^1P_1				9934.13	
2^1P_1				10296.07	
3^1P_1				10585.67	
4^1P_1				10837.38	
5^1P_1				11064.74	
6^1P_1				11274.68	

Chapter 9

SUMMARY AND CONCLUSIONS

Studies of meson mass spectra is one of the keys to understand the strong interaction between quarks. The strong interaction is mediated by massless particles called gluons. Since a meson is a simple two-body bound state of one quark and one anti-quark, meson mass spectroscopy provides a clue to the nature of the strong interaction and gives important hints about the behavior of gluons.

Studies of meson mass spectra in the context of constituent quark model was performed in this dissertation. The main goal of this research was to use relativistic kinematics and spin-dependent potentials to produce the meson mass spectra.

We studied the two-body Schrödinger equation in position, momentum and mixed representations. We studied the spinless Salpeter equation in mixed representation which is nothing but the Schrödinger equation with relativistic kinematics. Then we included spin-orbit and spin-spin interactions along with a linear confining potential and a Coulomb-like potential.

We used the variational principle to solve the equations numerically. We constructed the matrix eigenvalue equations and solved for the energies of mesons made of two heavy quarks. The main purpose of our work was to produce meson mass spectra with relativistic kinematics and spin-dependent potentials.

We produced meson mass spectra for heavy-heavy systems, $c\bar{c}$ and $b\bar{b}$. We used constituent quark masses for charm and bottom quarks. We produced the ground state and excited state energies of S $(l = 0, s = 0, 1)$, P $(l = 1, s = 0, 1)$ and D $(l = 2, s = 0, 1)$ states of $c\bar{c}$ and $b\bar{b}$. We used spectroscopic notation $n^{2s+1}L_j$ for the states where n is the principal quantum number, s is the total spin. L indicates the orbital angular momentum quantum number and j is the total angular momentum quantum number.

The meson masses predicted by our computations and the experimentally available meson masses were presented in the tables in previous chapter. The percentage error was calculated and presented for the cases where experimental masses were available.

From the results we clearly saw that the predicted mass values for heavy-heavy systems are close to the experimentally measured values.

Using relativistic kinematics and spin-dependent terms in the potential, we improved the values of predicted meson masses in the mass spectra. Previously relativity was handled with velocity dependent correction terms which involved many arbitrary constants [34] [16] [44] [51]. Previously spin effects were handled with many arbitrary interaction terms which also involved many arbitrary constants.[14] [9]

In our scheme, we used a mixed space formulation where relativistic kinematics was included directly into the equation. For the potential part, we used a linear plus a Coulomb-type potential along with a spin-spin interaction term and a spin-orbit interaction term. We had only three arbitrary constants to deal with, one for spin-spin term and other two for spin-orbit term of the potential. For the linear and Coulomb-type interactions, we used the Cornell parameters widely used by other researchers [16] [30] [52] [45]. So, in our computational scheme, we had fewer arbitrary constants and we predicted meson masses more accurately than some of the previous approaches.

Our predicted meson mass spectra and the comparison with experimental meson masses were presented in previous chapter. The success of our computational scheme to predict the meson mass spectra which are in good agreement with the experimental results encouraged us to extend our investigation towards fully relativistic treatment of the mesonic systems.

In conclusion, we presented theoretical and numerical techniques to study meson mass spectra in the context of quark-antiquark($q\bar{q}$) bound states. Meson mass spectra for heavy-heavy systems were produced using the constituent quark model. Relativistic kinematics was included in our equation. The potential we used were a linear plus a Coulomb-type potential along with the spin-dependent potentials. The linear constant σ and the Coulomb-type constant C were consistent with the values used by others.

The numerical approach we used was matrix formulation of the equation based on the variational principle. That method turned out to be a powerful method to construct matrix representation of the equations governing the two-body quark antiquark systems. We used orthonormal basis functions like Jacobi basis and Laguerre basis to construct our variational wavefunctions [42] [1].

We produced the meson masses up to the principal quantum number $n = 6$ for S, P and in some cases D states. We produced spin singlet($s = 0$) and spin triplets($s = 1$). We fit to the ground state and the xcited states were all predicted values. Our predicted values matched very well with the experimental values.

Appendix A

GRAM-SCHMIDT ORTHOGONALIZATION

A.1 Gram-Schmidt Procedure

This discussion about Gram-Schmidt procedure is taken from the paper of Charles et all.[53] The Gram-Schmidt orthonormalization method is typically introduced as a way to construct a set of orthonormal basis functions from a set of non-orthonormal basis functions. An orthonormal set makes computations in quantum mechanics much easier. [41] [40] [54]

The Gram-Schmidt procedure is easily implemented when only a few orthonormal basis functions are needed, but numerical techniques are usually employed when a larger set of orthonormal basis functions is needed. We present the analytical and numerical approach of constructing orthonormal basis functions via the Gram-Schmidt procedure and we discuss the limitations of the numerical approach.[53]

Before discussing orthonormalization, we first establish some notation. Let $\{|f_i\rangle\}$ be a set of column vectors and let $\langle f_i| = |f_i\rangle^\dagger$, where $|f_i\rangle^\dagger$ is the complex conjugate and transpose of $|f_i\rangle$. The scalar product is defined as $\langle f_i|f_j\rangle = \alpha$, where α is a real number. If the vectors $|f_i\rangle$ and $|f_j\rangle$ satisfy $\langle f_i|f_j\rangle = \delta_{ij}$, then these vectors are said to be orthonormal and the set $\{|f_i\rangle\}$ is an orthonormal set. The vector notation can be written in function language as

$$\langle r|f_i\rangle = f_i(r)$$

and

$$\langle f_i|f_j\rangle = \int_0^\infty f_i^*(r) f_j(r) dr \, .$$

Therefore, in function language, orthonormality means

$$\int_0^\infty f_i^*(r) f_j(r) dr = \delta_{ij} \, .$$

We are interested in orthonormalizing a set of functions $\{g_i(r)\}$ so that we obtain a new set $\{f_i(r)\}$ which is orthonormal according to the conditions above.

The Gram-Schmidt method is used to construct an orthonormal set of basis vectors $|f_i\rangle$ from a set of non-orthogonal but normalized basis vectors $|g_i\rangle$. Two arbitrarily positioned vectors $|g_1\rangle$ and $|g_2\rangle$ are chosen, which are normalized, but not orthogonal. $|g_1\rangle$ is chosen and set equal to $|f_1\rangle$.

We will construct vectors orthogonal to the new normalized basis vector $|f_1\rangle$. First, we construct another vector $|f_2\rangle$ which is orthogonal to $|f_1\rangle$. To do that, we use the vectors $|f_1\rangle$ and

$|g_2\rangle$. We project $\langle g_2|$ onto $|f_1\rangle$ giving the component of $|g_2\rangle$ that is parallel to $|f_1\rangle$. Now subtract from $|g_2\rangle$ the parallel component $\langle g_2|f_1\rangle$ along the $|f_1\rangle$ direction giving

$$|g_{2\perp}\rangle = |g_2\rangle - \langle g_2|f_1\rangle|f_1\rangle \; .$$

We label this orthogonal vector as $|g_{2\perp}\rangle$, since it is the component of $|g_2\rangle$ perpendicular to $|f_1\rangle$. Now that a vector orthogonal to $|f_1\rangle$ has been constructed, the next step is to find the normalization constant N_2 such that $|f_2\rangle = N_2|g_{2\perp}\rangle$,

$$|f_2\rangle = N_2\left(|g_2\rangle - \langle g_2|f_1\rangle|f_1\rangle\right) \; .$$

The normalization condition is $\langle f_2|f_2\rangle = 1$, so that

$$N_2^2\left(\langle g_2| - \langle f_1|g_2\rangle\langle f_1|\right)\left(|g_2\rangle - \langle g_2|f_1\rangle|f_1\rangle\right) = 1 \; ,$$

$$N_2^2\left(1 - \langle f_1|g_2\rangle^2\right) = 1 \; .$$

Thus, the normalization constant is

$$N_2 = \sqrt{\frac{1}{1-\langle f_1|g_2\rangle^2}} \; .$$

Now we construct a vector orthonormal to both $|f_1\rangle$ and $|f_2\rangle$ by using the same procedure,

$$|f_3\rangle = N_3\left[|g_3\rangle - \langle f_2|g_3\rangle|f_2\rangle - \langle f_1|g_3\rangle|f_1\rangle\right]$$

where

$$N_3 = \frac{1}{\sqrt{1-\langle f_2|g_3\rangle^2 - \langle f_1|g_3\rangle^2}} \; .$$

In general, we may construct a set of orthonormal basis $|f_n\rangle$ from a set of normalized but non-orthogonal basis $|g_n\rangle$ by using

$$|f_n\rangle = N_n\left[|g_n\rangle - \sum_{i=1}^{n-1} t_{in}|f_i\rangle\right] \; , \tag{A.1}$$

where

$$N_n = \sqrt{\frac{1}{1-\sum_{i=1}^{n-1} t_{in}^2}} \; , \tag{A.2}$$

and

$$t_{in} = \langle f_i|g_n\rangle \; .$$

A.2 Numerical Approach

We will construct the orthonormal basis functions $f_i(r)$ using the non-orthogonal, but normalized functions $g_i(r)$. We have shown that the orthonormal basis may be expressed in equation (A.1) as

$$|f_n\rangle = N_n \left[|g_n\rangle - \sum_{i=1}^{n-1} t_{in}|f_i\rangle \right] , \tag{A.3}$$

where

$$t_{in} = \langle f_i|g_n\rangle = \int_0^\infty f_i(r)g_n(r)dr ,$$

and the normalization is given by equation (A.2). As can be seen in equation (A.1), t_{in} should be computed before generating the orthonormal basis. Projecting $\langle g_j|$ onto equation (A.1) gives

$$\langle g_j|f_n\rangle = N_n \left[\langle g_j|g_n\rangle - \sum_{i=1}^{n-1} t_{in}\langle g_j|f_i\rangle \right] .$$

We define $G_{jn} \equiv \langle g_j|g_n\rangle$ and we project with $\langle g_j|$ onto equation (A.1) to obtain the recursive relation

$$t_{jn} = N_n \left[G_{jn} - \sum_{i=1}^{n-1} t_{in}t_{ij} \right] , \tag{A.4}$$

where $j > n > i$. An expression for G_{jn} is

$$G_{jn} = N_j^g N_n^g \frac{\sqrt{\pi}}{4(a_j + a_n)^{\frac{3}{2}}} , \tag{A.5}$$

where the normalization constants are given by equation (A.2). We note that since the functions $g(r)$ and $f(r)$ are real, $t_{in} = t_{ni}$ and $G_{in} = G_{ni}$. As described in the analytical approach, $|f_1\rangle = |g_1\rangle$. Next, calculate the elements in which $t_{j1} = G_{j1}$. Then, a general t_{jn} is calculated from equation(A.4) by iteration.

We can construct a matrix from the inner product of the orthonormalized basis functions,

$$D = \begin{pmatrix} \langle f_1|f_1\rangle & \langle f_1|f_2\rangle & \cdots & \langle f_1|f_m\rangle \\ \langle f_2|f_1\rangle & \langle f_2|f_2\rangle & \cdots & \langle f_2|f_m\rangle \\ \vdots & \vdots & \ddots & \vdots \\ \langle f_m|f_1\rangle & \langle f_m|f_2\rangle & \cdots & \langle f_m|f_m\rangle \end{pmatrix} , \tag{A.6}$$

where m is the total number of orthonormal basis functions. Since the matrix elements of D are $\langle f_i|f_j\rangle$,

$$\langle f_i|f_j\rangle = \int_0^\infty f_i(r)f_j(r)dr .$$

If $|f_i\rangle$ and $|f_j\rangle$ are indeed orthonormal, then D should be the identity matrix.

However, in practice, D will deviate from the identity matrix when a large number of functions is used.

The orthonormal basis functions were constructed numerically. The *analytical* functional forms of all of the orthonormal basis functions are not required. The advantage of the numerical approach is that one does not have to manipulate the cumbersome analytical functional forms. Since the basis functions were constructed numerically, one can compute the matrix elements of D and verify the orthonormality of $\langle f_i | f_j \rangle$ using a numerical integration method known as Gaussian Quadrature [42], which is discussed in Appendix B.

Appendix B

GAUSSIAN QUADRATURE

B.1 Gaussian Quadrature Method

This discussion about Gaussian Quadrature is taken from the paper Charles et. all. [53] Gaussian Quadrature is a very useful computational tool to perform the numerical integration. It approximates an integral as a sum as accurately as possible obeying the following relation:

$$\int_{-1}^{1} f(x)dx \approx \sum_{i=0}^{n-1} w_i f(x_i) \tag{B.1}$$

where f is the function of interest, x_i are the roots of the Legendre polynomials, n is the number of Gaussian points (number of roots of the Legendre polynomial) and w_i are the weights determined from the derivatives of the Legendre Polynomials evaluated at the roots using the relation stated below.

$$w_i = \frac{2}{(1-x_i^2)[P_i'(x_i)]^2} \tag{B.2}$$

where $P_i'(x_i)$ are the first derivatives of the Legendre Polynomials evaluated at the roots of the Legendre polynomials. Recursion relations stated below could be used to compute the first derivatives of the Legendre polynomials

$$P_0(x) = 1 \tag{B.3}$$

$$P_1(x) = x \tag{B.4}$$

and

$$(l+1)P_{l+1}(x) = (2l+1)xP_l(x) - lP_{l-1}(x) \tag{B.5}$$

Using the recursion relations,first derivatives of the Legendre Polynomials can be written as,

$$P_l'(x) = \frac{(l+1)P_l(x) - P_{l+1}(x)}{1-x^2} \tag{B.6}$$

The limits in the integrals must be transformed so that equation(B.1) is satisfied. That could be done by the suitable substitution of the variable. Let's suppose we have the following integral to evaluate,

$$\int_a^b f(x)dx \tag{B.7}$$

then it is required to make the following transformation

$$x' = mx + c \tag{B.8}$$

where $m = \frac{b+a}{2}$ and $c = \frac{b-a}{2}$ and $dx' = mdx$. So, we get

$$\int_a^b f(x)dx \to \int_{-1}^{1} f(x')dx' \approx \sum_{i=0}^{n-1} mw_i f(mx_i + c) \tag{B.9}$$

If we have an infinite integral of the following form,

$$\int_0^\infty f(x)dx \tag{B.10}$$

the following transformation is used to perform Gaussian quadrature:

$$x' = \tan\left[\frac{\pi}{4}(x+1)\right] \tag{B.11}$$

With the above substitution, $x' \to 0$ as $x \to -1$ and $x' \to \infty$ as $x \to 1$, so we obtain the following relation

$$\int_0^\infty f(x)dx \to \int_{-1}^{1} f(x')dx' \approx \sum_{i=0}^{n-1} f\left(\tan\left[\frac{\pi}{4}(x_i+1)\right]\right)\frac{\pi}{4}w_i \sec^2\left[\frac{\pi}{4}(x_i+1)\right] \tag{B.12}$$

After this proper transformation, we can apply Gaussian quadrature to evaluate the integral.

Other than tangent transformation, many other transformations are also possible. Depending on the particular problems to solve, the most suitable transformation is usually performed.

Appendix C

BASIS FUNCTIONS

C.1 Position-Space Basis Functions

The Gaussian and exponential basis functions are defined as,

$$g_i^G(r,b) = N_i^G r^{l+1} e^{-a_i r^2} \text{ where } N_i^G = \sqrt{\frac{2(2a_i)^{\frac{2l+3}{2}}}{\Gamma(\frac{2l+3}{2})}}, \tag{C.1}$$

and

$$g_i^E(r,b) = N_i^E r^{l+1} e^{-a_i r} \text{ where } N_i^E = \sqrt{\frac{(2a_i)^{2l+3}}{\Gamma(2l+3)}}. \tag{C.2}$$

The variational parameter is b and $a_i = (N_{max} b^2)/i^2$, where $i = 1,2,3,\ldots$ are the indices. The Laguerre basis functions are defined as

$$g_i^L(r,b) = \frac{(br)^{l+1}}{b\sqrt{N_i^L}} L_i^{2l+2}(2br) e^{-br}, \tag{C.3}$$

where $L_\alpha^\beta(x)$ are the Laguerre polynomials and the normalization is given by

$$N_i^L = b^{-3} \left(\frac{1}{2}\right)^{2l+3} \frac{\Gamma(i+2l+3)}{i!}. \tag{C.4}$$

The variational parameter is b and $i = 0,1,2,\ldots$ are the indices.[41] The Gaussian basis functions are not orthogonal,

$$\int_0^\infty g_i^G(r,b) g_j^G(r,b) dr = \frac{N_i^G N_j^G \Gamma(\frac{2l+3}{2})}{2(a_i+a_j)^{\frac{2l+3}{2}}}, \tag{C.5}$$

and the exponential basis functions are also not orthogonal,

$$\int_0^\infty g_i^E(r,b) g_j^E(r,b) dr = \frac{N_i^E N_j^E \Gamma(2l+3)}{(a_i+a_j)^{2l+3}}. \tag{C.6}$$

Since the Gaussian and exponential basis functions are not orthogonal, in order to use an orthonormal set we employ the Gram-Schmidt orthonormalization procedure. This procedure is discussed in Appendix A. The Laguerre basis functions [1] are orthonormal and they have the following property:

$$\int_0^\infty g_i^L(r,b) g_j^L(r,b) dr = \delta_{ij} \tag{C.7}$$

They form complete orthonormal set which we use in our computation for the mass spectra of the quantum mechanical two-body system.
The Harmonic Oscillator basis functions in position-space are given by

$$g_j^H(r,b) = N_{jl}\frac{r^l}{b^{l+1}}e^{-\frac{r^2}{2b^2}}L_{j-1}^{l+\frac{1}{2}}\left(\frac{r^2}{b^2}\right) \tag{C.8}$$

where N_{jl} is the normalization constant and is given by

$$N_{jl} = \sqrt{\frac{2(j-1)}{b\Gamma(j+l+\frac{1}{2})}} \tag{C.9}$$

The Harmonic Oscillator basis functions are orthonormal and satisfy the following property

$$\int_0^\infty g_i^H(r,b)g_j^H(r,b)dr = \delta_{ij} \tag{C.10}$$

They form complete orthonormal set which we use in our computation for meson mass spectra.

C.2 Momentum-Space Basis Functions

The Jacobi basis functions [1] in momentum-space are given as

$$g_j^J(p) = \frac{1}{\sqrt{N_{jl}}}\frac{(p/b)^l}{[(p/b)^2+1]^{l+2}}P_j^{(l+\frac{3}{2},l+\frac{1}{2})}\left[\frac{p^2-b^2}{p^2+b^2}\right], \tag{C.11}$$

where $P_j^{\alpha,\beta}(p/b)$ are the Jacobi polynomials and N_{jl} is

$$N_{jl} = \frac{b^3}{2(2j+2l+3)}\frac{\Gamma(j+l+\frac{5}{2})\Gamma(j+l+\frac{3}{2})}{j!\Gamma(j+2l+3)} \tag{C.12}$$

The Jacobi basis functions are orthonormal and satisfy the following property

$$\int_0^\infty g_i^J(p)g_j^J(p)dr = \delta_{ij} \tag{C.13}$$

They form complete orthonormal set which we use in our computation for meson mass spectra.
Note that the Laguerre and Jacobi basis functions are related by the Fourier-Bessel transform,

$$\tilde{g}(p) \quad = \sqrt{\tfrac{2}{\pi}}\int_0^\infty j_l(pr)g(r)r^2dr, \tag{C.14}$$

$$g(r) \quad = \sqrt{\tfrac{2}{\pi}}\int_0^\infty j_l(pr)\tilde{g}(p)p^2dp. \tag{C.15}$$

The Harmonic Oscillator basis functions in momentum-space are given by

$$g_j^H(p,b) = N_{jl}\frac{p^l}{b^{l+1}}e^{-\frac{p^2}{2b^2}}L_{j-1}^{l+\frac{1}{2}}\left(\frac{p^2}{b^2}\right) \tag{C.16}$$

where N_{jl} is the normalization constant and is given by

$$N_{jl} = \sqrt{\frac{2(j-1)}{b\Gamma(j+l+\frac{1}{2})}} \tag{C.17}$$

The Harmonic Oscillator basis functions are orthonormal and satisfy the following property

$$\int_0^\infty g_i^H(p,b) g_j^H(p,b) dr = \delta_{ij} \tag{C.18}$$

They form complete orthonormal set which we use in our computation for meson mass spectra.

BIBLIOGRAPHY

[1] M. Abramowitz and I.A. Stegun. *Handbook of Mathematical Functions*. Dover, Dover, New York, 1970.

[2] C. Amsler et al. Particle data group. *Physics Letters B*, 667, 2008.

[3] H. Hersbach. *Phys. Rev. D.*, 50, 1994.

[4] D. J. Gross and F. Wilczek. Ultraviolet behavior of non-abelian gauge theories. *Phys. Rev. Lett.*, 30, 1973.

[5] Francis Halzen and Alan D. Martin. *QUARKS AND LEPTONS: An Introductory Course in Modern Particle Physics*. John Wiley & Sons, 1984.

[6] David J. Griffiths. *Introduction to Elementary Particles*. John Wiley & Sons, Inc., 1987.

[7] M. Gell-Mann. *Phys. Rev. Lett.*, 8, 1964.

[8] C. Zweig. *CERN-TH-412*, 412, 1964.

[9] O.W.Greenberg. Spin and unitary-spin independence in a paraquark model of baryon and mesons. *Phys. Rev. Lett.*, 13, 1964.

[10] M. Han and Y. Nambu. *Phys. Rev. B.*, 139, 1965.

[11] R. P. Feynman. Very high-energy collisions of hadrons. *Phys. Rev. Lett.*, 23, 1969.

[12] J. D. Bjorken and E. A. Paschos. Inelastic electron-proton and γ-proton scattering and the structure of the nucleon. *Phys. Rev.*, 185, 1969.

[13] H. D. Politzer. Reliable perturbative results for strong interactions? *Phys. Rev. Lett.*, 30, 1973.

[14] K Hilnde R. Machleidt and Ch. Elster. *Phys. Rep.*, 1987.

[15] Olga Lakhina. *Study of Meson Properties In Quark Models*. PhD thesis, University of Pittsburgh, Pittsburgh, May 2008.

[16] N. Brambilla A Barchielli and G.M. Prosperi. Relativistic corrections to the quark-antiquark potential and the quarkonium spectrum. *IL Nuovo Cimento*, 103 A, 1990.

[17] P. Consoli N.Brambilla and G.M. Prosperi. Consistent derivation of the quark-antiquark and three-quark potentials in a wilson loop context. *Phys. Rev. D.*, 50, 1994.

[18] N.Brambilla and G.M. Prosperi. Flux tube model, quark-antiquark potentials and bethe-salpeter kernel. *Phys. Rev. D.*, 47, 1993.

[19] N. Brambilla. On the form of quark-qntiquark bethe-salpeter kernel. *Nuovo Cimento*, 105 A:949, 1992.

[20] Frank Wilczek. *The Lightness of Being*. Basic Books, New York, 2008.

[21] C.D. Roberts and A. G. Williams. Dyson-schwinger equations and the application to hadronic physics. *Prog. Part. Nucl. Phys.*, 33, 1994.

[22] Ming-Qiu and Dao-Wei Wang. Light cone qcd sum rules for the semileptonic decay $\lambda \rightarrow pl\bar{\nu}$. *Phys. Rev. D*, 69, 2004.

[23] T. Kopaleishvili. *Bound $q\bar{q}$ systems in the framework of different versions of 3D reductions of the Bethe-Salpeter equation*. PhD thesis, Tbilisi State University, University St. 9, 380086 Tbilisi, Geogia, February 2008.

[24] F. Mandl and G. Shaw. *QUANTUM FIELD THEORY*. John Wiley & Sons Ltd., 1984.

[25] Khin Maung Maung, David E. Kahana, and John W. Norbury. Solution of two-body relativistic bound-state equations with confining plus coulomb interactions. *Phys Rev D.*, 47:1182, 1993.

[26] Khin Maung Maung, John W. Norbury, and David E. Kahana. Regge trajectories from the two-body, bound-state thompson equation using a quark-confining interaction in momentum space. *Phys Rev D.*, 48:3408, 1993.

[27] John W. Norbury, David E. Kahana, and Khin Maung Maung. Confining potential in momentum space. *Can. J. Phys.*, 70(1):86–89, 1992.

[28] John W. Norbury, Khin Maung Maung, and David E. Kahana. Numerical tests of the lande subtraction method for the coulomb potential in momentum space. *Phys Rev A.*, 50:2075, 1994.

[29] J. R. Spence and J. P. Vary. Solving momentum-space integral equations for quarkonia spectra with confining potentials. ii. *Phys. Rev. D.*, 35, 1987.

[30] Z. Chen L.P. Fulcher and K.C. Yeong. Energies of quark-antiquark systems, the cornell potential, and the spinless salpeter equation. *Phys. Rev. D.*, 47, 1993.

[31] L.P. Fulcher. Structure of light meson multiplets and a semirelativistic model. *Phys. Rev. D.*, 34, 1986.

[32] L.P. Fulcher. Phenomenological prediction of properties of the b_c system. *Phys. Rev. D.*, 60, 1999.

[33] L.P. Fulcher. Matrix representation of the nonlocal kinetic energy operator, the spinless salpeter equation and the cornell potential. *Phys. Rev. D.*, 50, 1994.

[34] S. G. Bankova. Light meson masses in the local approximation of the schrödinger equation with relativistic kinematics. *J. Phys. G: Nuclear Part. Phys.*, 19:1143–1154, 1993.

[35] V.O. Galkin D.Ebert, R.N. Faustov and W. Lucha. *Phys. Rev. D*, 76, 2007.

[36] A.V. Tatarinstev R.N. Faustov, V.O.Galkin and A.S.Vshivstev. Algebric approach to the spectral problem for the schrödinger equation with power potential. *Int. J. Mod. Phys. A*, 15, 2000.

[37] Mitcel Weissbluth. *Atoms and Molecules*. Academic Press Inc., New York 10003, 1978.

[38] Charles M. Werneth, Mallika Dhar, Khin Maung Maung, Christopher Sirola, and John W. Norbury. Variational method using basis functions. *J.Phys.A: Math Theor*, 43, 2010.

[39] Ernest S. Abers. *Quantum Mechanics*. PEARSON EDUCATION INC.,Upper Saddle River, New Jersey 07458.

[40] R.E. Larson and B.H. Edwards. *Elementary Linear Algebra*. Toronto: Heath and Company, 1991.

[41] G.B. Arfken and H. J Webber. *Mathematical Methods for Physicists*. San Diego: Academic Press, 1995.

[42] S.A. Teukolsky W.H. Press, B. P. Flannery and W.T. Vetterling. *Numerical Recipes*. Cambridge: Cambridge University Press, 1990.

[43] B.D. Keister and W. N. Polyzou. Useful bases for problems in nuclear particle physics. *J. Comp. Phys.*, 134(2), 1997.

[44] D. Robson H.C. Jean and A.G. Williams. Relativistic quark-antiquark bound-state problem with spin-dependent interactions in momentum space. *Phys. Rev. D.*, 50, 1994.

[45] M. Rotenberg. *Ann. Phys.*, 19, 1961.

[46] E. Eichten and F. Feinberg. Spin-dependent forces in quantum chromodynamics. *Phys. Rev. D*, 23, 1981.

[47] D. Gromes. *Z. Phys. C*, 26, 1984.

[48] D. Gromes. Spin dependent forces between quarks, preprint. *HD-THEP-87-16*, 1987.

[49] D.P. Stanley and D. Robson. Nonperturbative potential model for light and heavy quark-antiquark systems. *Phys. Rev. D.*, 21, 1980.

[50] Wei-Shu Hou and Gwo-Guang Wong. Glueball spectrum from a potential model. *Physical Review D*, 67, 2003.

[51] S. Godfrey and N. Isgar. Mesons in a relativized quark model with chromodynamics. *Phys. Rev. D.*, 32, 1985.

[52] B. Durand and L. Durand. Connection of relativistic and nonrelativistic wave functions in the calculation of leptonic widths. *Phys. Rev. D.*, 30, 1984.

[53] Charles M. Werneth, Mallika Dhar, Khin Maung Maung, Christopher Sirola, and John W. Norbury. Numerical gram-schmidt orthonormalization. *Eur.J.Phys.*, 31, 2010.

[54] R. Shankar. *Principles of Quantum Mechanics*. New York: Plenum, 1994.